A mechanosensory system governs myosin II accumulation in dividing cells

Yee-Seir Kee[a,b], Yixin Ren[a], Danielle Dorfman[a], Miho Iijima[a], Richard Firtel[c], Pablo A. Iglesias[d], and Douglas N. Robinson[a,e,f]

[a]Department of Cell Biology, Johns Hopkins University School of Medicine, Baltimore, MD 21205; [b]Department of Biophysics, Johns Hopkins University, Baltimore, MD 21218; [c]Section of Cell and Developmental Biology, University of California, San Diego, La Jolla, CA 92093; [d]Department of Electrical and Computer Engineering, Johns Hopkins University, Baltimore, MD 21218; [e]Department of Pharmacology and Molecular Sciences, Johns Hopkins University School of Medicine, Baltimore, MD 21205; [f]Department of Chemical and Biomolecular Engineering, Johns Hopkins University, Baltimore, MD 21218

ABSTRACT **The mitotic spindle is generally considered the initiator of furrow ingression. However, recent studies suggest that furrows can form without spindles, particularly during asymmetric cell division. In *Dictyostelium*, the mechanoenzyme myosin II and the actin cross-linker cortexillin I form a mechanosensor that responds to mechanical stress, which could account for spindle-independent contractile protein recruitment. Here we show that the regulatory and contractility network composed of myosin II, cortexillin I, IQGAP2, kinesin-6 (kif12), and inner centromeric protein (INCENP) is a mechanical stress–responsive system. Myosin II and cortexillin I form the core mechanosensor, and mechanotransduction is mediated by IQGAP2 to kif12 and INCENP. In addition, IQGAP2 is antagonized by IQGAP1 to modulate the mechanoresponsiveness of the system, suggesting a possible mechanism for discriminating between mechanical and biochemical inputs. Furthermore, IQGAP2 is important for maintaining spindle morphology and kif12 and myosin II cleavage furrow recruitment. Cortexillin II is not directly involved in myosin II mechanosensitive accumulation, but without cortexillin I, cortexillin II's role in membrane–cortex attachment is revealed. Finally, the mitotic spindle is dispensable for the system. Overall, this mechanosensory system is structured like a control system characterized by mechanochemical feedback loops that regulate myosin II localization at sites of mechanical stress and the cleavage furrow.**

Monitoring Editor
Carole Parent
National Institutes of Health

Received: Jul 6, 2011
Revised: Feb 15, 2012
Accepted: Feb 24, 2012

INTRODUCTION

More than a century of research has indicated that cytokinesis contractility is generally regulated by the mitotic spindle (Wolpert, 1966; Hiramoto, 1990; Rappaport, 1996; Burgess and Chang, 2005). Components of these regulatory pathways include the kinesin-6 proteins that form complexes with signaling proteins such as MgcRacGap, which regulates the Rho pathway, or the chromosomal passenger complex proteins (inner centromeric protein [INCENP] and aurora kinase; Cooke *et al.*, 1987; Glotzer, 2005; Li *et al.*, 2008). The *Dictyostelium* kinesin-6 (also known as kif12), INCENP, and aurora kinase localize to the central spindle and the cleavage furrow at later stages of cytokinesis (Chen *et al.*, 2007; Li *et al.*, 2008). Although these pathways are believed to modulate the cortex mechanics that promote cytokinesis shape change, disruption or removal of the spindle after chromosome separation does not affect cytokinesis in at least some cell types (Hiramoto, 1956; von Dassow *et al.*, 2009). In addition, the mitotic spindle may not be the primary director of contractility during asymmetric cell divisions (Cabernard *et al.*, 2010; Ou *et al.*, 2010). Thus cytokinesis contractility is regulated by multiple mechanochemical pathways (Surcel *et al.*, 2010), which undoubtedly promote cytokinesis

This article was published online ahead of print in MBoC in Press (http://www.molbiolcell.org/cgi/doi/10.1091/mbc.E11-07-0601) on February 29, 2012.

Address correspondence to: Douglas N. Robinson (dnr@jhmi.edu).

Abbreviations used: CIT, citrine fluorescent protein; CM, contractile machinery composed of cortexillin I and myosin II; ΔBLCBS, a short-lever-arm myosin II with both light-chain–binding sites deleted; 2xELC, a long-lever-arm myosin II with an extra essential light-chain–binding site; GFP, green fluorescent protein; I_c, mean intensity of the cytoplasm; $I_{f\ center}$, mean intensity at the furrow center; I_f/I_p, mean intensity at the furrow cortex/mean intensity at the polar cortex; $I_{p\ cyto}$, mean intensity at the polar cytoplasm; I_p/I_o, mean intensity of the cortex inside the pipette/mean intensity of the opposite cortex; mCh, mCherry fluorescent protein; MPA, micropipette aspiration; RFP, red fluorescent protein; SEM, standard error of the mean; T_{eff}, effective cortical tension; WT, wild type.

fidelity and versatility in order to maintain genomic stability (Fujiwara *et al.*, 2005).

One critical component of the cytokinesis machinery is the force-sensitive, actin-binding mechanoenzyme myosin II. Since the classic experiments of Fenn and Huxley (Fenn, 1923; Huxley and Simmons, 1971), myosin II has been well understood to be load sensitive, and this load sensitivity is at the crux of how various muscle tissues function across diverse physiological processes. However, given that muscle is a late evolutionary arrival, it has been unclear how this force sensitivity might contribute to cytokinesis dynamics and perhaps promote contractility in the absence of obvious spindle cues. To begin to address this question, we previously tested whether dividing *Dictyostelium* cells respond to applied mechanical stress and whether this sensitivity relies on the load-dependent nature of the myosin II motor domain. Indeed, dividing cells are exquisitely sensitive to applied mechanical stress. The mechanosensor consists of at least three parts: the myosin II motor itself with force amplification through the lever arm, the dynamics of myosin II bipolar thick filament assembly/disassembly, and actin filament anchoring through cortexillin I (Effler *et al.*, 2006; Ren *et al.*, 2009). A physical model confirms that the mechanical stress–sensitive cooperative binding of myosin II to actin is sufficient to mediate myosin's cellular mechanosensitive accumulation (Luo *et al.*, 2012). In particular, the cellular mechanosensory response can be accounted for quantitatively based on the assumptions that myosin II cooperatively binds actin filaments in the isometric state (Orlova and Egelman, 1997; Tokuraku *et al.*, 2009) and that myosin II binding to actin filaments enhances bipolar thick filament assembly (Mahajan *et al.*, 1989).

Dictyostelium and mammalian bipolar thick filament assembly/disassembly dynamics is regulated by heavy chain phosphorylation (Egelhoff *et al.*, 1993; Bosgraaf and van Haastert, 2006; Breckenridge *et al.*, 2009). In contrast, cortexillin I regulation at the molecular level is much less well understood. Cortexillin I may interact with rac1 through IQGAP1 (also known as DGap1) and IQGAP2 (also known as GapA; Faix *et al.*, 1998, 2001; Lee *et al.*, 2010; Mondal *et al.*, 2010). Cortexillin II, which is 60% identical in amino acid sequence to cortexillin I, does not appear to interact with IQGAP proteins. In contrast to *cortexillin I* (*cortI*)-null cells, *cortexillin II* (*cortII*)-null cells also do not exhibit an apparent cytokinesis phenotype (Faix *et al.*, 1996; Mondal *et al.*, 2010). On the other hand, IQGAP2 is essential for cytokinesis, as cells depleted of IQGAP2 fail to divide and are highly multinucleated (Adachi *et al.*, 1997). The role of IQGAP1 in cytokinesis remains elusive, but it is believed to regulate the actin cytoskeleton (Faix *et al.*, 1998). In mammals, IQGAP proteins interact with the microtubule plus-end–binding protein CLIP-170 upon activation of rac1 and cdc42 and links microtubules to the actin cytoskeleton network in fibroblasts (Fukata *et al.*, 2002). However, whether IQGAP regulates microtubule-based signaling pathways—specifically the ones emanating from the mitotic spindle in dividing cells—is less clear. Nevertheless, all of these observations point to different key components that play roles in cytokinesis. Integration of these pieces of information is required to understand how cytokinesis is regulated with high fidelity.

In this study, we characterized a mechanosensory system that fine-tunes the level of myosin II and cortexillin I at the cleavage furrow to facilitate division under various mechanical contexts. This mechanosensory system consists of the mechanical stress–induced, self-amplifying recruitment mechanism of myosin II and cortexillin I, which form the core mechanosensor module of the system. Mechanical stress is detected by the mechanosensor, which then triggers the accumulation of mitotic spindle signaling proteins kif12 and INCENP through IQGAP2. However, IQGAP2, kif12, and INCENP are not required for myosin II mechanosensitive localization. Therefore the IQGAP2, kif12, and INCENP accumulation reflects the conversion of the mechanical stress sensed by myosin II into their redistribution, and we refer to this form of mechanosensitive accumulation as mechanotransduction. We also uncover a complex relationship between IQGAP1 and IQGAP2, where IQGAP1 acts as an inhibitor of the mechanosensor. IQGAP2 is needed to relieve this inhibition. Cortexillin II is not required for mechanosensing, although *cortexillin I/II* (*cortI/II*) double mutants have severe membrane–cortex attachment defects, implying a role for cortexillin II in maintaining membrane–cortex attachment. Overall, IQGAP2, kif12, INCENP, and the mechanosensor proteins concentrate myosin II at the cleavage furrow. Thus this mechanosensory system is composed of multiple feedback loops, which may ensure the flexibility and high fidelity of cytokinesis.

RESULTS

Mechanical stress recruits kif12 and INCENP

Although spindle signals direct the contractile machinery (CM; specifically cortexillin I and myosin II) to initiate furrow formation (Cooke *et al.*, 1987; Glotzer, 2005; Li *et al.*, 2008), mechanical stress can also direct the recruitment of the CM (Effler *et al.*, 2006; Ren *et al.*, 2009). Therefore we tested whether the mechanical stress has any effect on spindle signaling molecules. Because *Dictyostelium* cells do not have MgcRacGAP or Rho kinase, we focused on kinesin 6 (kif12), INCENP, and aurora kinase (Lakshmikanth *et al.*, 2004; Chen *et al.*, 2007; Li *et al.*, 2008). We expressed green fluorescent protein (GFP)–tagged kif12, INCENP, and aurora kinase in WT cells. On application of mechanical stress using micropipette aspiration (MPA), kif12 and INCENP, but not aurora kinase, accumulated at the deformation site in a similar manner to the myosin II mechanosensitive response (Figure 1A). The accumulation of kif12 and INCENP was significantly higher than the intensity ratio (I_P/I_o = 0.82) of soluble GFP or mCherry, which reflects the volume (thickness) ratio between the portion of the cell inside the micropipette as compared with the opposing cortex (Figure 1A, dot plot). The recruitment of kif12 to the mechanically stressed region is myosin II dependent because in *myosin II* (*myoII*)-null cells, kif12 failed to accumulate at the micropipette (Figure 1B). Kif12 accumulation is also independent of the mitotic spindle. After ~5 min of 10 μM nocodazole treatment, which disrupts the spindle, kif12 still accumulated to the micropipette (Figure 1B). Because kif12 and INCENP, as well as myosin II and cortexillin I, can be recruited to the mechanically deformed cortex, we examined whether kif12 and INCENP are required for myosin II mechanosensitive localization. In the absence of either kif12 or INCENP, myosin II was recruited to the deformation site at wild-type (WT) levels (Figure 1C). Furthermore, the *kif12* and *incenp* mutants had nearly normal cortical tension (Figure 1D). These results imply that although kif12 and INCENP undergo mechanosensitive accumulation, they are neither required for mechanosensing nor crucial for cortical tension maintenance. Therefore mechanical stress is detected by the mechanosensory module formed by myosin II and cortexillin I and transmitted downstream to recruit kif12 and INCENP as part of a mechanotransduction pathway (Figure 1E).

IQGAP2 maintains mechanosensitivity in the presence of IQGAP1

Cortexillin I is one central component of the mechanosensory module. Cortexillin I is believed to localize to the cleavage furrow by forming complexes with rac1 (encoded by three nearly identical genes—*rac1A*, *B*, and *C*), IQGAP1, and IQGAP2 (Faix *et al.*, 1998, 2001; Lee *et al.*, 2010; Mondal *et al.*, 2010). To see how cortexillin I

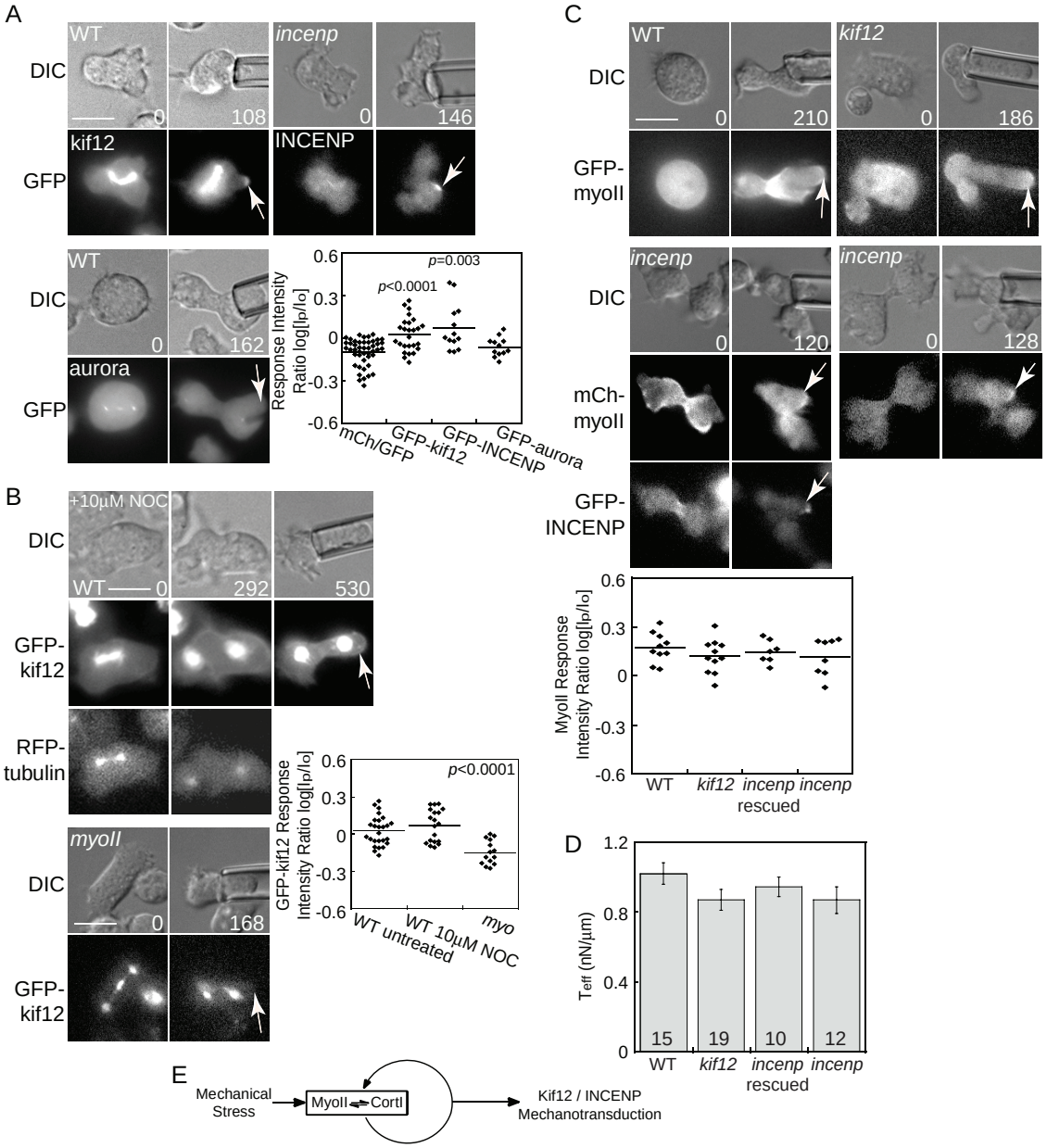

FIGURE 1: Kinesin-6 (kif12) and INCENP are directed to cortical regions of high mechanical stress in a myosin II–dependent and microtubule-independent manner but are not required for myosin II mechanosensitive accumulation. (A) GFP-kif12 and GFP-INCENP, but not GFP-aurora, localized to sites of mechanical deformation induced by micropipette aspiration of dividing WT or rescued cells (arrows). The graph shows the GFP-tagged protein response ($\log[I_P/I_o]$, where I_P is the intensity in the pipette and I_o is the intensity of the opposite cortex) in WT and rescued cells. The distributions of GFP-kif12 and GFP-INCENP response intensity ratio in WT and rescued cells are significantly higher than in WT cells expressing either GFP or mCherry alone (Student's *t* test: $p < 0.0001$) and cells expressing GFP-aurora (Student's *t* test: $p = 0.003$). The distribution of GFP-aurora is not different from that of GFP/mCherry (Student's *t* test: $p = 0.14$). Each dot represents an aspirated cell. The numbers in the differential interference contrast images represent the start of the movie (time 0 s) and the time of the response after the pressure was applied. (B) GFP-kif12 accumulated at the micropipette independent of microtubules but dependent on myosin II. Cells were treated with 10 μM nocodazole (NOC), and the RFP-tubulin was monitored to confirm that the mitotic spindle was disrupted. The response distribution of GFP-kif12 in *myoII*-null cells is significantly lower than in the untreated (reproduced from A) and 10 μM nocodazole-treated cells (ANOVA: $p < 0.0001$). Note that the bright spherical structures shown in GFP-kif12 images are the centrosomes. (C) GFP-myosin II mechanosensitive accumulation occurred similarly in WT vs. *kif12*-null cells and *incenp*-rescued vs. *incenp*-null cells. The distributions are statistically indistinguishable (WT and *kif12* null, Student's *t* test: $p = 0.22$; *incenp* rescued and *incenp* null, Student's *t* test: $p = 0.53$). Scale bars (A–C), 10 μm. (D) The effective cortical tension (T_{eff}) of *kif12* and *incenp* null cells was only slightly reduced compared with WT and GFP-INCENP–rescued controls (Student's *t* test: $p = 0.08$ and 0.67, respectively). Sample sizes are listed on the bar graph. (E) Cartoon summarizes the data in this figure. Mechanical stress directs the recruitment of myosin II and cortexillin I, which in turn are required to direct mechanosensitive accumulation (mechanotransduction) of kif12 and INCENP.

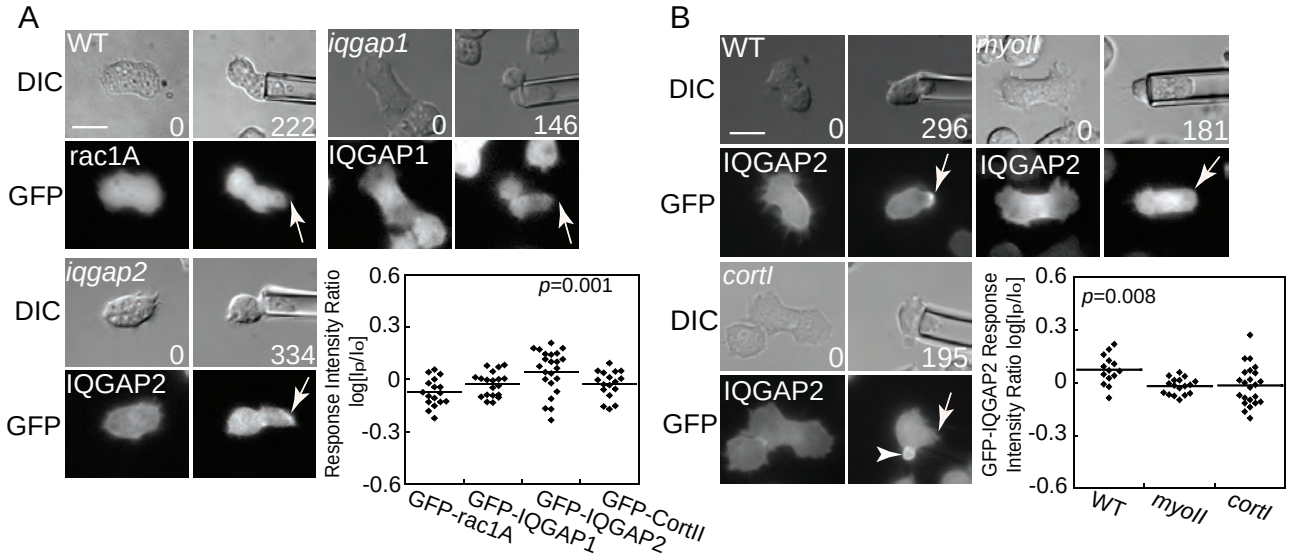

FIGURE 2: IQGAP2 is sensitive to mechanical stress in a manner dependent on myosin II and cortexillin I. (A) Of the cortexillin I regulators rac1A, IQGAP1, IQGAP2, and cortexillin II expressed in WT or complemented mutant (*iqgap1*, *iqgap2*, *cortII*) strains, only IQGAP2 is recruited to the micropipette in dividing cells. The IQGAP2 response magnitude is significantly higher than that of rac1A, IQGAP1, and cortexillin II (ANOVA: $p = 0.001$). (B) IQGAP2 does not accumulate at the micropipette in *myoII*- or *cortI*-null cells (white arrows; ANOVA: $p = 0.008$). Note that *cortI*-mutant cells, which form a lot of blebs, showed strong accumulation of IQGAP2 at the blebs (arrowhead). Scale bars,10 μm.

might be regulated in mechanosensing, we examined the regulators of cortexillin I, as well as of cortexillin II, to see whether they are recruited in response to mechanical stress. We expressed GFP-tagged rac1A in WT cells and GFP-cortexillin II, GFP-IQGAP1, and GFP-IQGAP2 in *cortII*-, *iqgap1*-, and *iqgap2*-null cells, respectively. Performing MPA on dividing cells, we found that IQGAP2, but not cortexillin II, IQGAP1, or rac1A, accumulated at the deformation site (Figure 2A). We also obtained similar results when we expressed GFP-IQGAP1 and GFP-IQGAP2 in WT cells (Supplemental Figure S1A and Figure 2B). Both myosin II and cortexillin I were required for the recruitment of IQGAP2 to the micropipette (Figure 2B). Moreover, we observed that IQGAP2 strongly accumulated at blebs (arrowhead in Figure 2B) in *cortI*-null cells, which have a less stable cortex.

We then tested whether cortexillin II, rac1, IQGAP1, and/or IQGAP2 are required for myosin II mechanosensitive accumulation by examining GFP-myosin II in *cortII*-, *rac1A/C* double-mutant (the *rac1A/B/C* triple mutants appear to be inviable), and *iqgap1*- and *iqgap2*-null cells. Myosin II mechanosensitivity was defective in *iqgap2*-null cells but remained normal in *cortII*, *rac1A/C*, and *iqgap1* mutants (Figure 3A, images and dot plot). When the *iqgap2* mutant was complemented with GFP-IQGAP2, myosin II mechanosensing was restored to WT levels (Figure 3B). Initially, one might conclude that IQGAP2 is required for myosin II mechanosensing. However, it is also possible that IQGAP1 and IQGAP2 act antagonistically to regulate mechanosensitivity but are not part of the mechanosensory module. Therefore we measured myosin II mechanosensitive localization in *iqgap1/2* double-mutant cells and found that the myosin II accumulation was WT like in this strain (Figure 3A). IQGAP2 then is not an integral part of the mechanosensory module but instead suppresses IQGAP1-mediated inhibition of myosin II mechanosensitive localization. Consistently, overexpression of GFP-IQGAP1 in WT cells, which still express endogenous IQGAP1, suppressed myosin II–mediated mechanosensing (Figure 3B). Furthermore, *iqgap1/2* double-mutant cells expressing GFP-IQGAP2 had normal myosin II mechanosensitive localization. On the other hand, expression of GFP-IQGAP1 in the double mutant inhibited myosin II mechanosensitive localization (Supplemental Figure S1B). In addition, cortexillin I responded similarly to myosin II in *rac1A/C*, *iqgap1*, *iqgap2*, and *iqgap1/2* mutant cells (Figure 3C). Overall, these results are consistent with the notion that cortexillin I and myosin II constitute the mechanosensory module and are both regulated by the IQGAPs.

When we checked myosin II recruitment in *cortI/II* double-mutant cells, the I_P/I_o intensity ratio showed no difference as compared with WT (Figure 3A, dot plot, Student's *t* test: $p = 0.41$). However, *cortI/II* cells have a less stable cortex–membrane attachment, resulting in recruitment of myosin II to blebs and dramatic membrane–cortex rupture sites inside or outside the pipette (Supplemental Figure S2A). Because IQGAP2 localized strongly to blebs in *cortI* null cells (Figure 2B), we checked whether IQGAP2 also accumulates at the blebs of *cortI/II* null cells. We found that indeed IQGAP2 localizes to blebs in the *cortI/II* mutant cells, and the I_P/I_o intensity ratio did not show a significant difference from WT (Supplemental Figure S2B). Given the level of membrane–cortex rupture observed in nearly every *cortI/II* mutant cell analyzed, this mode of myosin II mechanosensitive localization is different from that in the rest of the mutant cell lines we characterized. In addition, cortexillin II is not required for cortexillin I mechanosensitive localization, which was verified by analyzing GFP-cortexillin I expressed in *cortI/II* mutant cells (Figure 3C, dot plot). Thus cortexillin II does not appear to play a direct role in the myosin II– and cortexillin I–mediated mechanosensitive localization.

Finally, we measured the cortical tension of all of these mutant cell lines (Figure 3D). The IQGAPs are important for cortical tension maintenance: cortical tension was reduced by 35, 60, and 80% in *iqgap1*, *iqgap2*, and *iqpgap1/2* nulls, respectively. The *cortII* cells had a slight 16% increase in cortical tension. The cortical tension was reduced by 35 and 60% in *cortI* and *cortI/II*, respectively. These results demonstrate that the changes in mechanosensitivity do not simply correlate with changes in cortical tension levels.

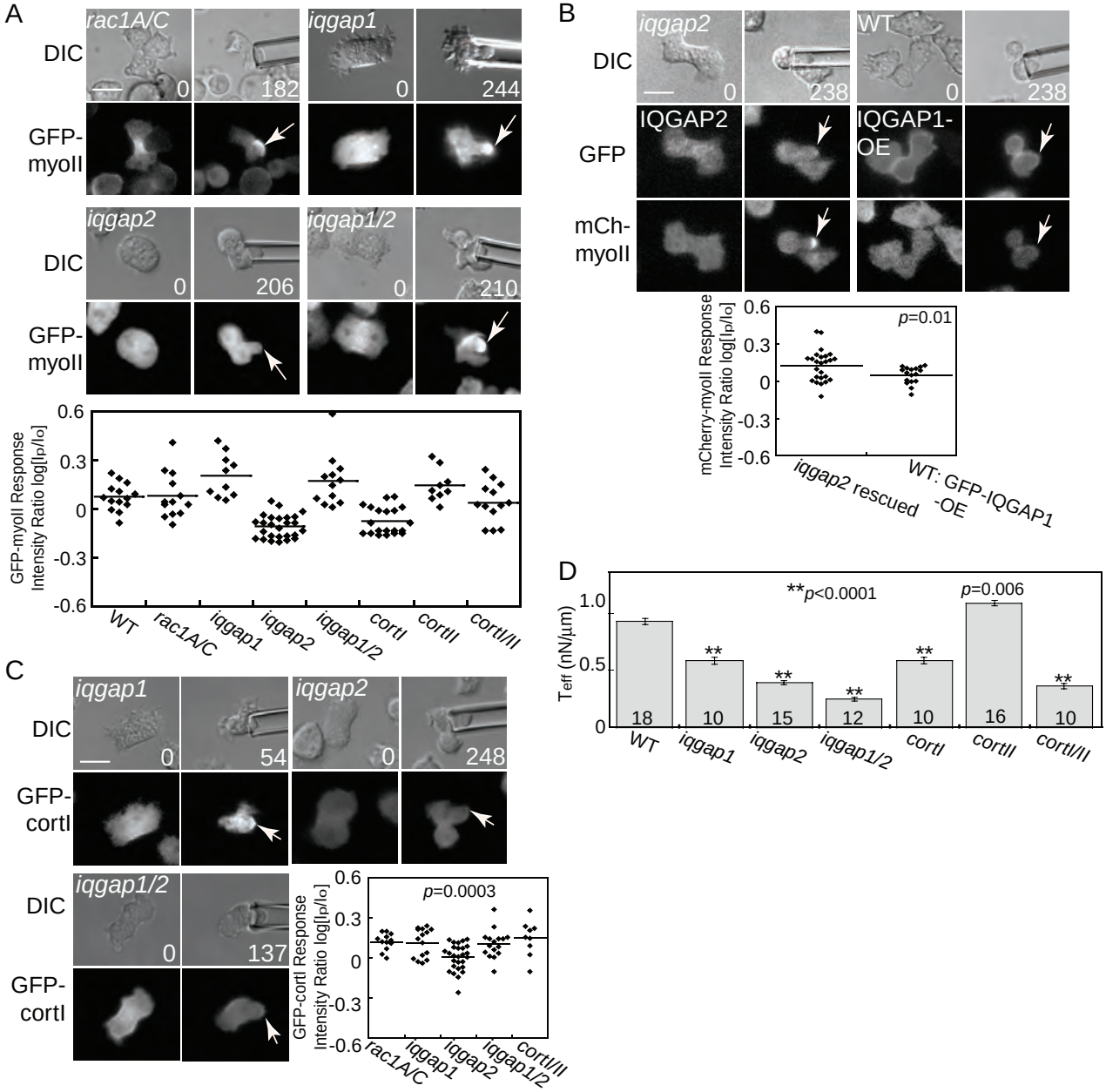

FIGURE 3: Roles of IQGAP proteins in mechanosensitivity regulation and cortical tension. (A) GFP-myosin II showed WT levels of mechanosensitive accumulation in *rac1A/C* double mutants, *cortII* single mutants, and *iqgap1/2* double mutants (Student's *t* test: p = 0.9, 0.1, and 0.07, respectively) but not *iqgap2* and *cortI* single mutants (Student's *t* test: p < 0.0001 for both cases). GFP-myosin II responsiveness is higher in *iqgap1* null cells than in WT (Student's *t* test: p = 0.01). Although GFP-myosin II recruitment in *cortI/II* is not statistically different from WT (Student's *t* test: p = 0.4), the recruitment behavior is not WT like (see Supplemental Figure S2). (B) Rescue of *iqgap2* cells with IQGAP2 restored the myosin II mechanosensitive accumulation, whereas IQGAP1 overexpression in WT cells inhibited myosin II mechanosensitive accumulation (Student's *t* test: p = 0.01). (C) Cortexillin I showed a similar dependence as myosin II on IQGAP function. Cortexillin I accumulated in *iqgap1* and *iqgap1/2* and *cortI/II* mutants but not in *iqgap2* single-mutant cells (ANOVA: p = 0.0003). Scale bars (A, C), 10 μm. (D) The effective cortical tension of WT, *iqgap1*, *iqgap2*, *iqgap1/2*, *cortI*, *cortII*, and *cortI/II* mutant cells. Each strain is significantly different from WT (and each other; Student's *t* test: p < 0.0001 for all except *cortII*, p = 0.006). Sample sizes are listed on the bar graph.

Kif12 mechanosensitive accumulation and cleavage furrow localization depend on IQGAP2

In the preceding sections, we found that kif12 accumulation at the mechanically stressed cortex is myosin II dependent, and IQGAP2 maintains myosin II and cortexillin I mechanosensing by suppressing IQGAP1. Therefore IQGAP2 could mediate the mechanosensitive accumulation of kif12. Indeed, the level of GFP-kif12 recruitment to the micropipette is significantly lower in the *iqgap2* mutants than in the WT parental cells (Figure 4A). Because myosin II mechanosensitive accumulation in the *iqgap2* mutant is suppressed but in the *iqgap1/2* double-mutant cells is active, we tested whether having active myosin II mechanosensing is sufficient to trigger the

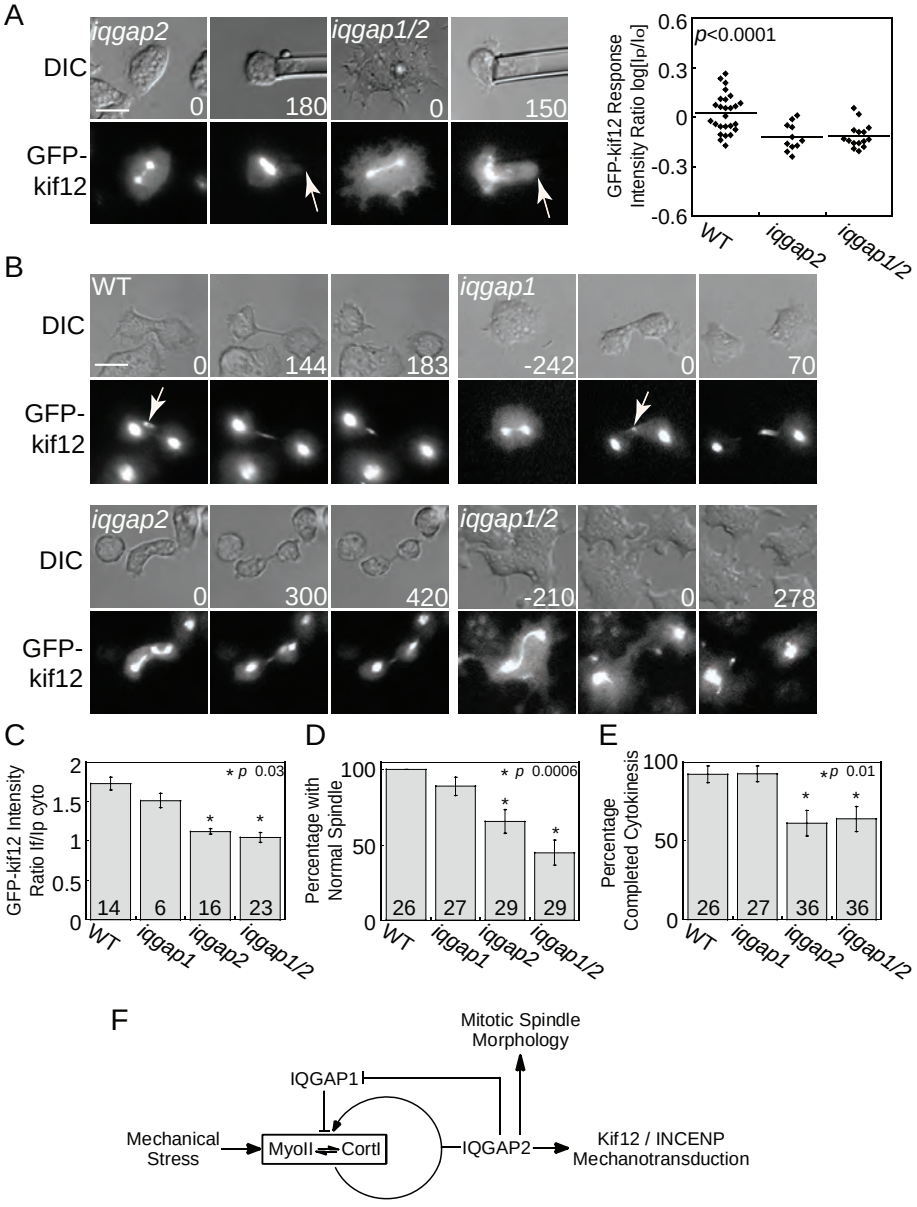

FIGURE 4: Mechanosensitive and cleavage furrow accumulation of kif12 and normal spindle morphology requires IQGAP2. (A) GFP-kif12 recruitment was deficient in *iqgap2*- and *iqgap1/2*-null cells. WT control data were redrawn from Figure 1A. The difference between the WT control and the *iqgap* single and double mutants was significant (ANOVA: $p < 0.0001$). (B) WT and *iqgap1*-null cells had normal spindle morphology and cleavage furrow localization of GFP-kif12 (white arrows). The *iqgap2*- and *iqgap1/2*-null cells had disrupted spindle morphology, and GFP-kif12 furrow localization was reduced or absent. Scale bars (A, B), 10 µm. (C) The quantification of the intensity ratio of GFP-kif12 at the furrow to polar cytoplasm ($I_f/I_{p\ cyto}$). The $I_f/I_{p\ cyto}$ values in WT and *iqgap1* cells were indistinguishable (Student's *t* test: $p = 0.44$). The intensity ratio was significantly lower in *iqgap2* (Student's *t* test: $p = 0.03$) and *iqgap1/2* (Student's *t* test: $p = 0.02$) cells as compared with WT cells. (D) The percentage of *iqgap2* and *iqgap1/2* null cells with normal spindles was much lower than that in WT and *iqgap1* (comparison of proportions: $p \leq 0.0006$). (E) The *iqgap2* and *iqgap1/2* mutants were deficient in cytokinesis, as the percentage of cells completing cytokinesis was much lower than for WT and *iqgap1*-null cells (comparison of proportions: $p \leq 0.006$). The sample sizes for C–E are listed on the bar graphs. (F) Cartoon summarizes data from this figure and Figures 1–3. Mechanical stress detected by the myosin II/cortexillin I mechanosensor is transduced through IQGAP2 to kif12 and INCENP. IQGAP2 is also important for maintaining normal spindle morphology and is required to suppress IQGAP1, which inhibits mechanosensing.

recruitment of kif12. In the absence of both IQGAP1 and IQGAP2, kif12 failed to be recruited to the micropipette despite having active myosin II mechanosensitive accumulation (Figure 4A). By coexpressing GFP-kif12 and mCherry-myosin II in the *iqgap1/2* mutants so that both proteins could be tracked simultaneously, we further confirmed that myosin II, but not kif12, showed active mechanosensitive localization in these double-mutant cells (Supplemental Figure S1C).

Because kif12 in *iqgap2* and *iqgap1/2* mutants failed to be recruited by mechanical stress, we then determined whether the kif12 levels at the cleavage furrow depended on IQGAP2. We compared the mean intensity ratio of GFP-kif12 at the furrow to that at the polar cytoplasm ($I_f/I_{p\ cyto}$) in WT, *iqgap1*, *iqgap2*, and *iqgap1/2* cells (Figure 4B). WT and *iqgap1*-mutant cells showed higher GFP-kif12 levels at the furrow than at the polar cytoplasm (Figure 4, B and C). Conversely, *iqgap2* and *iqgap1/2* mutants showed little GFP-kif12 at the furrow (Figure 4, B and C). Thus IQGAP2 is required for kif12 accumulation at the mechanically stressed cortex and at the cleavage furrow.

We observed other cell division defects in the *iqgap2*, *iqgap1/2*, and *kif12* mutants. The *iqgap2* and *iqgap1/2* cells had more severe spindle morphological defects than did WT and *iqgap1* cells (Figure 4, B and D). The percentage of cells that completed cytokinesis was also much lower in *iqgap2* and *iqgap1/2* mutant cells than in WT and *iqgap1* cells (Figure 4E). In contrast, we did not see spindle morphological defects in the *kif12* mutant ($n = 9$) or its WT parental cell line ($n = 22$), although *kif12* mutant cells did show severe defects in cytokinesis completion (with 2 of 14 cells vs. 32 of 32 WT cells completing cytokinesis). Cytokinesis in *kif12* cells was usually arrested at the stage at which a thin intercellular bridge connected the two daughter cells, and this bridge often fused back to form binucleated cells. Thus spindle morphology by itself does not simply correlate with cytokinesis success in these strains. Overall, these results highlight the central role of IQGAP2 in maintaining normal mitotic spindle morphology and serving as a mediator that transmits mechanical signals detected by the CM mechanosensor to kif12 (Figure 4F).

Normal myosin II cleavage furrow accumulation requires only IQGAP2 when cells are dividing unperturbed on surfaces

Because our goal is to define the network that regulates myosin II accumulation at the cleavage furrow, we quantified the mean furrow-to-pole intensity ratio of GFP-myosin II in WT and mutant cells undergoing cytokinesis unperturbed on surfaces. To simplify the analysis, we focused on cells in which the furrows had ingressed

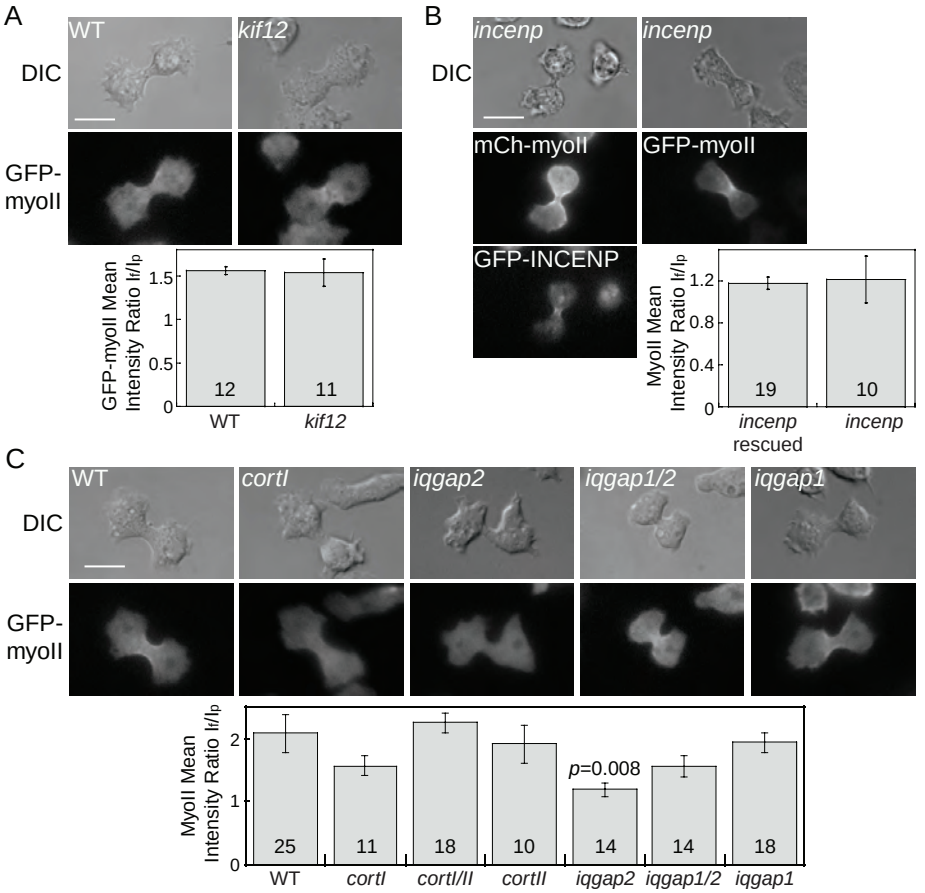

FIGURE 5: Myosin II cleavage furrow accumulation is significantly reduced in unperturbed *iqgap2*-null cells. (A) In cells grown on surfaces (without perturbation), GFP-myosin II accumulated at the cleavage furrow at comparable levels in WT and *kif12*-null cells. (B) GFP-myosin II levels at the cleavage furrow were similar in *incenp*-rescued cells and *incenp*-null cells. (C) Images of GFP-myosin II in WT, *cortI*, *iqgap1*, *iqgap2*, and *iqgap1/2* cells grown on surfaces. By pairwise analysis of each mutant as compared with the WT control, only the *iqgap2* null is significantly lower (Student's *t* test: p = 0.008). Scale bars, 10 μm. The bar graphs show the mean furrow-to-pole intensity ratio ($I_f/I_p \pm$ SEM), and the sample sizes are listed on the bars.

to around the crossover distance D_x, which is where the furrow length and diameter are equal and the myosin II amounts have plateaued (Zhang and Robinson, 2005; Ren *et al.*, 2009). In *kif12*- and *incenp*-null cells, the myosin II furrow-to-pole intensity ratio (I_f:I_p) is comparable to the I_f:I_p ratio of both WT and the *incenp* rescued cells (Figure 5, A and B, graphs). Thus kif12 and INCENP are not required for myosin II accumulation when cells divide unperturbed on surfaces.

We then analyzed *cortI*, *cortII*, *iqgap1*, and *iqgap2* single- and double-mutant cells to determine whether they show alterations in myosin II furrow accumulation. Only the *iqgap2*-null mutant cells showed a statistically significant reduction in myosin II accumulation at the cleavage furrow when they divided unperturbed on surfaces (Figure 5C, graph). Of interest, compared with WT cells, the *cortI*-null cells had slightly reduced but statistically indistinguishable myosin II levels at the cleavage furrow. This could be due to the existence of cortexillin II. Therefore we checked the furrow localization of cortexillin II in the absence of cortexillin I by expressing GFP-cortexillin II in *cortI/II* null cells. Indeed, cortexillin II localized to the cleavage furrow in these cells, as well as in the *rac1A/C* mutants (Supplemental Figure S3). However, the important role of the IQGAPs and the distinct regulation of cortexillin II were further highlighted by the observation that cortexillin II did not show significant cleavage furrow enrichment in *iqgap1/2*-null cells, even though these cells did localize myosin II (Supplemental Figure S3 and Figure 5C).

Because only the *iqgap2* mutants showed a significant reduction in myosin II levels at the cleavage furrow, simply examining unperturbed cells dividing on surfaces may not reveal the full richness of the systems that regulate myosin II accumulation. Therefore another assay is required to mechanically challenge the dividing cells to determine how these pathways synergize to regulate myosin II cleavage furrow accumulation.

Cortexillin I, IQGAP2, kif12, and INCENP are required for normal myosin II cleavage furrow accumulation under global mechanical stress

Yumura *et al*. (1984) demonstrated that dividing cells gently compressed under a thin layer of agarose showed a significant increase in myosin II localization at the cleavage furrow We used this method of applying a uniform two-dimensional global mechanical stress to cells and analyzed the I_f:I_p ratios. First, we assayed soluble GFP, which was uniformly distributed throughout the cytoplasm and had an unchanged I_f:I_p ratio under agarose overlay (Supplemental Figure S4). This confirms that the changes from compression by agarose overlay detailed later are not simply due to the imaging of flattened cells. After this test, we examined fluorescent protein–labeled myosin II in WT cells and each of the various mutant cell types characterized earlier.

In WT cells, GFP-kif12 rescued *kif12*-null cells and GFP-INCENP rescued *incenp*-null cells, the myosin II I_f:I_p ratio increased threefold to sevenfold over uncompressed cells. The *kif12* and *incenp* mutants showed little or no increase in this ratio under agarose overlay compared with the unperturbed state (Figure 6, A and B). This ratio could increase if I_f goes up, I_p goes down, or a combination of the two occurs. Therefore we measured the polar-to-cytoplasm intensity ratio (I_p/I_c) and found that these were significantly different between these strains (e.g., WT I_p/I_c = 0.93 ± 0.06 vs. *kif12* I_p/I_c = 1.2 ± 0.1; Student's *t* test: $p = 0.02$). This rise of polar myosin II in the *kif12* and *incenp* mutants was expected because the myosin II localization in these cells is still mechanoresponsive (Figure 1C). However, this amount of polar myosin II increase was not sufficient to account for the decrease in the I_f/I_p ratio, indicating the kif12 and INCENP focus myosin II at the furrow in response to mechanical stress. These results support the role of spindle signaling proteins kif12 and INCENP in directing myosin II localization to the cleavage furrow.

Because kif12 recruitment to the deformation site induced by MPA is mitotic spindle independent (Figure 1B) and previously we found that myosin II mechanosensing does not require the mitotic spindle (Effler *et al*., 2006), we tested whether the strong myosin II enhancement at the cleavage furrow under agarose overlay is also spindle independent. We labeled the WT cells with GFP–myosin II

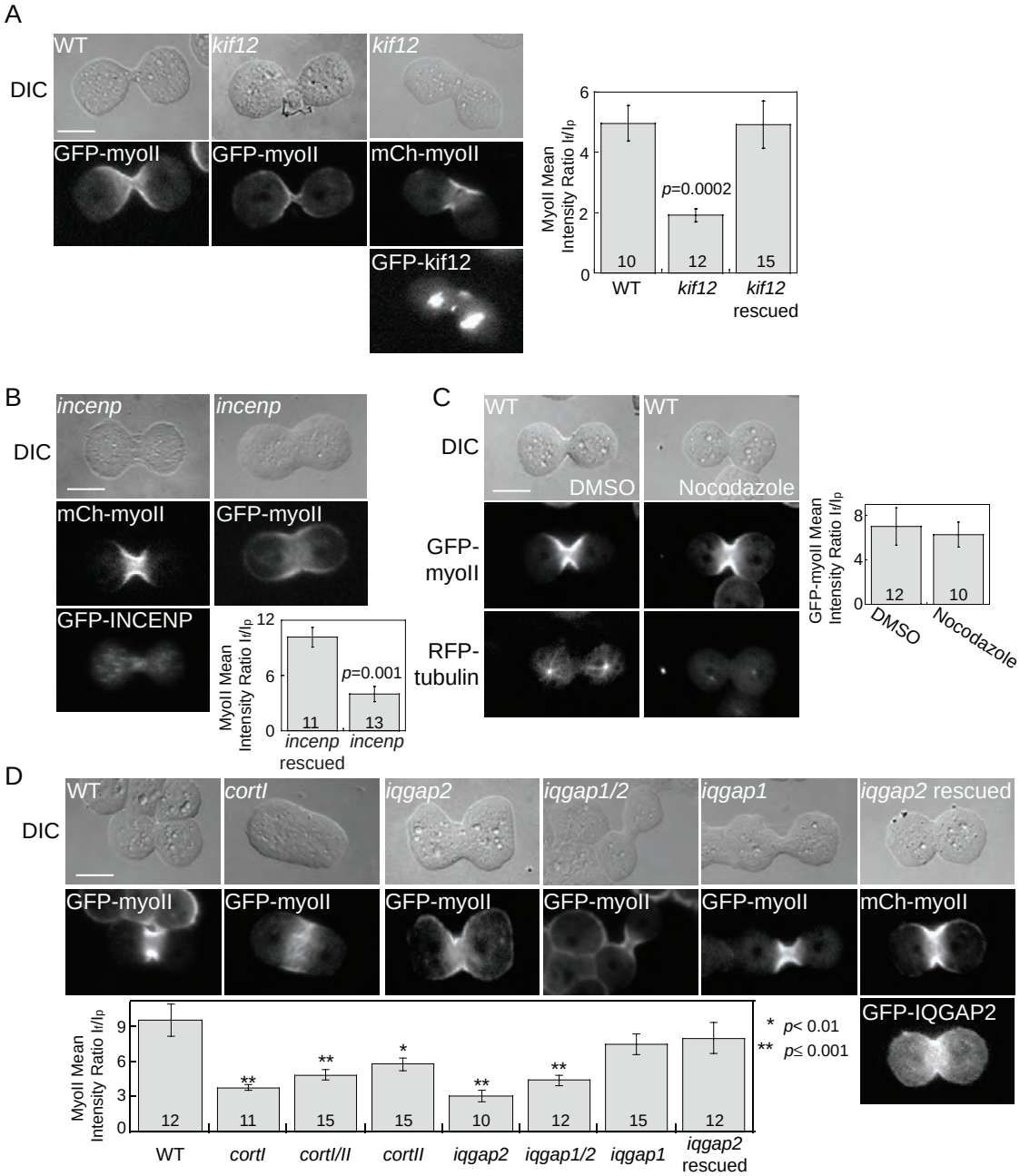

FIGURE 6: Mechanically challenged cells require kif12, INCENP, cortexillin I, and IQGAP2 for normal myosin II accumulation. (A) On agarose overlay, the myosin II levels at the cleavage furrow increased threefold in WT and *kif12*-rescued cells (as compared with unperturbed cells; Figure 5A). This amplification was lost in *kif12*-null cells (Student's *t* test: p = 0.0002). (B) INCENP was required for stress-induced amplification of myosin II accumulation at the cleavage furrow cortex. Under agarose overlay, the rescued *incenp* cell line showed threefold higher myosin II accumulation than the *incenp*-null cells had (Student's *t* test: p = 0.001). (C) WT cells treated with the DMSO carrier and WT cells treated with 10 μM nocodazole showed comparable accumulation of myosin II in response to agarose overlay. The spindle was confirmed to be disrupted by tracking RFP-tubulin. (D) Except for *iqgap1*- and *iqgap2*-rescued cells, all mutants showed significant differences in the GFP-myosin II I_f/I_p ratios as compared with WT cells. Statistical analysis was performed using an ANOVA with a Student Neuman–Keuls post hoc test. The p values are indicated in the inset, and level of significance is indicated with asterisks. Scale bars, 10 μm. The bar graphs show the mean furrow-to-pole intensity ratio ($I_f/I_p \pm$ SEM), and the sample sizes are listed on the bars.

and red fluorescent protein (RFP)–tubulin so that the spindle could be tracked. Dividing cells were first treated with 10 μM nocodazole and monitored until the spindles were disassembled. Cells were then compressed by agarose overlay. These dividing cells had a similar level of GFP–myosin II I_f:I_p ratio as the dimethyl sulfoxide (DMSO)–treated control cells (Figure 6C). Therefore the mechanical stress–induced recruitment of myosin II to the cleavage furrow is mitotic spindle independent.

Next we quantified the GFP–myosin II levels at the cleavage furrow in the WT, single and double *cortexillin* mutant, and single and

double *iqgap* mutant cells under agarose overlay. In contrast to cytokinesis on surfaces where only the *iqgap2*-null cells showed a statistically significant reduction in cleavage furrow myosin II, a much richer set of differences and trends was observed with agarose overlay. Without IQGAP2 (analysis of variance [ANOVA]: $p < 0.0001$) or cortexillin I ($p = 0.0002$), the GFP–myosin II I_f:I_p ratio is about one-third of WT levels (Figure 6D). In the *iqgap1/2*-null cells, the GFP–myosin II I_f:I_p ratio was slightly higher than in the *iqgap2* and *cortI* single mutants (Figure 6D). This ratio for *iqgap1/2*-null cells, however, is still much lower than that of WT ($p = 0.0006$) and *iqgap2* cells rescued with GFP-IQGAP2 ($p = 0.03$; Figure 6D). The I_f:I_p ratio in *cortII* nulls is significantly lower than in WT (70% of WT; $p = 0.008$) but is not significantly different from that in *iqgap2*-rescued cells (Figure 6D, $p = 0.13$). In the absence of both cortexillin I and II, the I_f:I_p ratio is about half of the WT level ($p = 0.0008$). Finally, the *iqgap1* single-mutant cells had a GFP–myosin II I_f:I_p ratio comparable to that of WT and *iqgap2*-rescued cells (Figure 6D). Thus, by perturbing components that control myosin II mechanosensing and kif12/INCENP mechanosensitive accumulation, we observed predictable changes in the levels of myosin II recruitment to the cleavage furrow. These results suggest that the mechanosensory system helps tune the myosin II levels at the cleavage furrow cortex.

Force amplification through the myosin II lever arm is important for concentrating myosin II at the lateral cleavage furrow cortex and for modulating furrow ingression dynamics

Finally, we used one more approach to test whether myosin II mechanosensitivity contributes to cleavage furrow amplification due to global mechanical stress. One of the central ideas about the myosin II–based mechanosensory system is that myosin II binds actin cooperatively in the isometric state and accumulates at sites of mechanical stress (Ren *et al.*, 2009; Tokuraku *et al.*, 2009; Uyeda *et al.*, 2011; Luo *et al.*, 2012). Previous studies demonstrated that this principle applies to myosin II mechanosensing by analyzing the myosin II recruitment in *myoII*-null cells rescued with either WT myosin II (with the normal essential light-chain- and regulatory light-chain–binding sites), a long-lever-arm myosin II with an extra essential light-chain–binding site (2xELC), or a short-lever-arm myosin II with both light-chain–binding sites deleted (ΔBLCBS). The pressure dependence of the mechanical stress–induced accumulation correlated inversely with the motors' lever arm lengths (i.e., the longer the lever arm, the lower is the stress required to drive accumulation; Ren *et al.*, 2009). This observation indicates that myosin accumulates because the motor stalls on the actin in response to stress.

To verify whether the mechanosensitive property of myosin II is important for the stress-induced amplification of the myosin levels at the cleavage furrow, we explored how ΔBLCBS myosin II responds to the uniform mechanical stress from agarose overlay. We found that accumulation of citrine (CIT)-labeled ΔBLCBS in the furrow region is not significantly different from that of CIT-WT myosin II under agarose compression (both myosins were expressed in *myoII*-null cells labeled with GFP-tubulin; Figure 7, A and B). However, ΔBLCBS did not concentrate at the lateral edges of the cleavage furrow cortex as strongly as WT myosin II did. This observation is reflected in the line-scan graphs and the intensity ratios of the furrow edges relative to the furrow center ($I_f/I_{f\ center}$; Figure 7, A and C) and was verified by confocal microscopy (Supplemental Figure S5A). Thus the WT myosin II lever arm is required for the lateral cortex concentration at the cleavage furrow, which is predicted to be the region with the highest cortical tension (Liu *et al.*, 1996). These observations are also consistent with an earlier agarose overlay study showing that the nonhydrolyzer myosin II mutant (without ATPase and motor activity) localized at the cleavage furrow region but failed to be concentrated at the lateral edges of the cleavage furrow cortex (Yumura and Uyeda, 1997). Thus full myosin II function and mechanosensing correlate with myosin II's ability to incorporate strongly at the lateral cleavage furrow cortex.

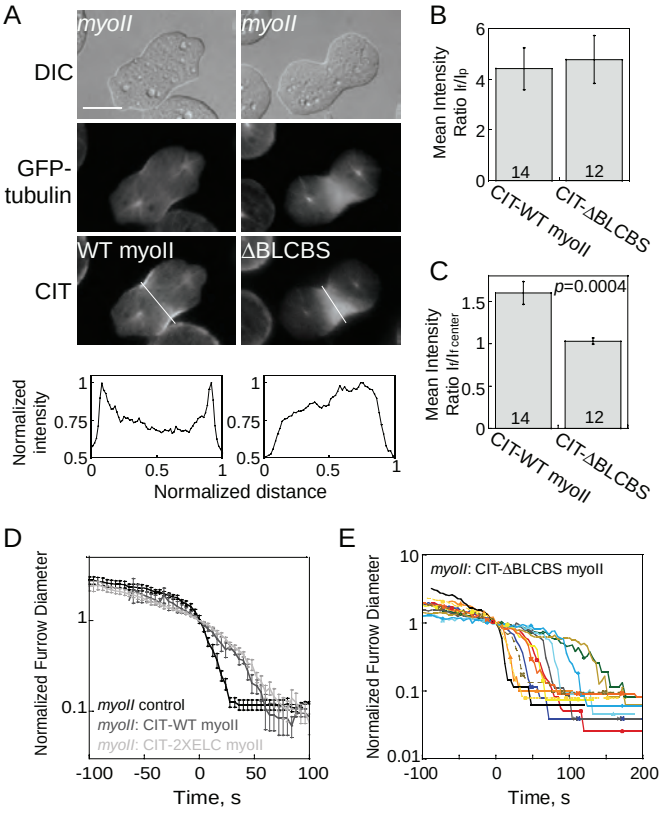

FIGURE 7: WT myosin II lever arm determines cleavage furrow cortex concentration and furrow ingression dynamics. (A) Citrine (CIT)-labeled WT and ΔBLCBS myosin II (expressed in GFP-tubulin-labeled *myoII*-null cells) accumulated at the cleavage furrow under agarose overlay, but ΔBLCBS did not integrate as tightly at the lateral edges of the cleavage furrow cortex. Line scans at the line in the fluorescence images show the distribution of myosin II in the cortex vs. the central region of these furrows. Scale bar, 10 μm. A comparison by confocal microscopy is presented in Supplemental Figure S5A. (B) The bar graph shows the quantification of the mean furrow-to-pole intensity ratio of (I_f/I_p) of CIT-WT and CIT-ΔBLCBS myosin II (Student's *t* test: $p = 0.77$). (C) The bar graph shows the quantification of the mean ratio of lateral furrow cortex to furrow center ($I_f/I_{f\ center}$) of CIT-WT and ΔBLCBS myosin II (Student's *t* test: $p = 0.0004$). Sample sizes are shown on the bar graphs in B and C. (D, E) The graphs depict the furrow-thinning dynamics of *myoII*-null cells (black line) and *myoII*-null cells complemented with a CIT-labeled WT myosin II (gray line), long-lever-arm 2xELC myosin II (light gray line), and the short-lever-arm ΔBLCBS myosin II. (D) The WT and 2xELC myosin II, which had indistinguishable furrow ingression dynamics, whereas *myoII* cells showed accelerated furrow thinning. (E) Individual ΔBLCBS furrow ingression dynamics were similar to those of *myoII*-null cells, but they failed to collapse onto a single universal curve. Unaveraged *myoII*-null, WT, and 2xELC curves are given in Supplemental Figure S5, B–D.

Finally, we returned to unperturbed cells to test whether the lever arm affects cleavage furrow ingression dynamics (Zhang and Robinson, 2005; Reichl *et al.*, 2008). We measured the furrow

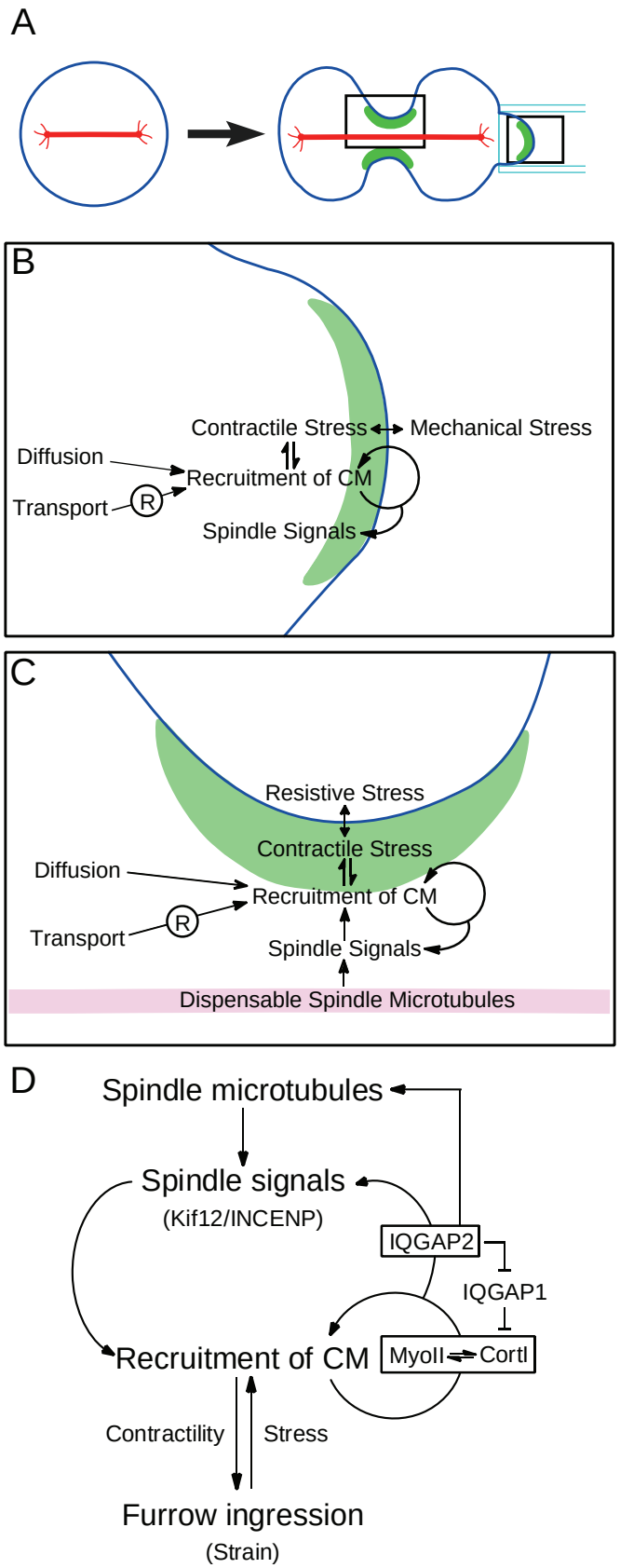

FIGURE 8: Model for how a control system regulates CM recruitment at sites of mechanical stress, including the cleavage furrow. (A) The mitotic spindle (red line) elongates as the symmetry of the round, dividing cell is broken and the contractile machinery (CM) composed of cortexillin I and myosin II begins to accumulate at the mid zone, initiating furrow formation (green patch at the cleavage furrow; see C for detail view). On micropipette aspiration, CM, which constitutes the mechanosensor module, is recruited to the mechanically stressed cortex (green patch inside the micropipette; see B for a detailed view). (B) Mechanical stress—for example, by micropipette aspiration—recruits CM, which generates contractile stress to counteract the applied mechanical stress. The mechanical stress detected by the mechanosensor then leads to the accumulation of spindle signaling proteins. The mitotic spindle is dispensable for both CM mechanosensing and the mechanosensitive accumulation of spindle signaling proteins. Other mechanisms, such as diffusion, active transport, and/or cortical receptor (R) binding, also contribute to CM accumulation. (C) During cleavage furrow ingression, CM is recruited to the cleavage furrow cortex by spindle signals from spindle microtubules (MTs) and CM mechanosensing induced by mechanical stress such as from contractility, which acts against the resistive stress at the furrow. Diffusion and active transport and/or cortical receptor binding also contribute to CM accumulation. If the MTs are disrupted, myosin II can still be recruited to the cleavage furrow. The control system may also be engaged by the mechanical stress generated by the CM as it pulls against the viscoelastic cortex. (D) Schematic, depicting the control system that tunes the level of myosin II at the cleavage furrow cortex. The system may be activated by the spindle and/or mechanical stress. Cortexillin I and myosin II define the core mechanosensor. IQGAP2 antagonizes IQGAP1 to maintain an active mechanosensory module, and IQGAP2 mediates mechanosensitive localization of kif12 and INCENP. IQGAP2 also plays a role in maintaining morphology of the mitotic spindle.

ingression dynamics of *myoII*-null cells and *myoII*-null cells rescued with CIT-labeled WT, 2xELC, or ΔBLCBS myosin II proteins. We found an inverse relationship between the rates of furrow ingression and the lever arm length. Furrows of cells expressing WT and the 2xELC were slower than the *myoII*-null furrows during late stages of furrow ingression (Figure 7D and Supplemental Figure S5, B–D). Cells expressing ΔBLCBS myosin II showed *myoII* null–type dynamics, but these furrow-thinning trajectories did not collapse onto a single universal curve (Figure 7E). Instead, they showed a broad range of times at which the furrow ingression dynamics transitioned to the fast, final furrow-thinning phase. These observations support the notion that the WT and 2xELC myosin II motors are experiencing mechanical stress and operating near stall during furrow ingression (Zhang and Robinson, 2005; Reichl *et al.*, 2008). This mechanical stress may then trigger a mechanosensory control system to tune the myosin II levels (Figure 8).

DISCUSSION

Many biological tasks, ranging from allosteric protein–protein interactions and immune function to information flow in the brain that governs human behavior, rely on a control system that automatically ensures proper function in the presence of disturbances or perturbations (Monod *et al.*, 1963; Tucker and Williamson, 1984; Takahashi and Yamada, 1998). These control systems rely on feedback to maintain quasi-equilibrium or homeostasis. Such a feedback control system has also been characterized in motility regulation in mammalian cells, which requires the synergistic coupling of F-actin, myosin II, and focal adhesion dynamics (Gupton and Waterman-Storer, 2006).

The network described here also has the hallmark of a control system (Figure 8). As the mitotic cell enters anaphase, the spindle elongates and delivers initial cues, which stimulate cleavage furrow formation (Figure 8A). Cells respond to applied mechanical stresses

(similar in magnitude to those generated at the cleavage furrow; Zhang and Robinson, 2005) by recruiting CM to generate counteracting contractile stress, thereby modulating the localization of spindle signaling proteins (Figure 8B). In addition, this mechanosensory system appears to function at the cleavage furrow. After breaking the symmetry of the dividing cells, spindle microtubules, along with contractile stress in the cortex, drive CM recruitment to the cleavage furrow cortex (Figure 8C). The control system is sensitive to mechanical perturbations, such as the intrinsic stress that a cell normally experiences at the cleavage furrow or from external stresses imposed by the environment, which significantly amplify myosin II levels (Figure 8D). The amplification occurs at two places: myosin II/cortexillin I–mediated mechanosensing and then mechanosensitive accumulation of kif12 and INCENP mediated by IQGAP2. The baseline of cleavage furrow myosin II in both unperturbed and compressed states is found in the *iqgap2* single-mutant cells. These *iqgap2* mutants also failed to shows myosin II mechanosensing and kif12/INCENP mechanosensitive accumulation. The addition of mechanosensation (*iqgap1/2* double mutants) increases myosin II cleavage furrow levels ~1.5-fold when applying compressive stress (as compared with the *iqgap2*-mutant baseline under compression). Overall, the intact WT system amplifies myosin II levels approximately fivefold in the presence mechanical stress. This amplification, along with the continuously increasing rates of myosin II accumulation in response to mechanical stress, suggest the presence of a feedback loop, a hallmark of many control systems (Ren *et al.*, 2009; Luo *et al.*, 2012).

This control system works as part of, or alongside, other modes of CM targeting, which include diffusion, active transport, regulatory factors, and/or cortical receptors (Zang and Spudich, 1998; Yumura *et al.*, 2008; Fang *et al.*, 2010; Uehara *et al.*, 2010; Laporte *et al.*, 2011). If the spindle microtubules are disrupted after the dividing cell elongates, the contractile stress at the furrow, along with the mechanosensory control system, are sufficient to ensure adequate recruitment of CM. The spindle independence suggests that the control system might account for how cells divide under diverse mechanical constraints and in the absence of a mitotic spindle (Hiramoto, 1956; Cabernard *et al.*, 2010; Ou *et al.*, 2010).

We discovered an intricate relationship between cortexillin I–interacting proteins IQGAP1 and IQGAP2. Neither IQGAP is essential for mechanosensing; however, IQGAP2 is required for kif12/INCENP mechanosensitive recruitment and to counteract the inhibition by IQGAP1, allowing mechanosensing to occur. These observations suggest a mechanism by which different signals—biochemical and mechanical—may be discriminated by a similar set of cytoskeletal proteins. The inhibition by IQGAP1 may also dampen the system, preventing it from being overly sensitive to mechanical inputs. Moreover, IQGAPs are found to be important for maintaining normal cell mechanics, and IQGAP2 specifically is crucial for cytokinesis. It is also known that IQGAP1 and 2 interact with the C and N-termini of cortexillin I, respectively (Faix *et al.*, 1996; Mondal *et al.* 2010). The N-terminus of cortexillin I consists of a calponin-homology actin-binding domain, whereas the C-terminus is important for actin bundling and lipid binding (Stock *et al.*, 1999). Previously, we found that the N-terminus of cortexillin I is dispensable, but the C-terminus including the coiled-coil domain is essential, for myosin II mechanosensitive localization (Ren *et al.*, 2009). Cortexillin I may be trapped in a nonmechanosensitive conformation when IQGAP1 interacts with its C-terminus. On the other hand, IQGAP2 may enable cortexillin I mechanosensitivity by interacting with its N-terminus, freeing up the C-terminus for myosin II–mediated mechanosensing and actin and lipid binding. Perhaps in this conformation, cortexillin I is more effective at transmitting mechanical stress from the plasma membrane to the actin cortex, which may promote myosin II's mechanosensitivity. It is significant that IQGAPs are becoming central players in cell division in a variety of organisms. For example, budding and fission yeast IQGAP proteins are crucial for anchoring myosin II at the division site (Fang *et al.*, 2010; Laporte *et al.*, 2011). IQGAP2 clearly plays a central role in the control system described here and may constitute one of the myosin II cortical anchors in *Dictyostelium* as well (Robinson, 2010).

Unlike cortexillin I, cortexillin II does not seem to be directly involved in the mechanosensory system, as it does not localize in response to mechanical stress. Cortexillin II does contribute to cortical tension and stability, as the *cortI/II* double mutants display a much reduced cortical tension and higher levels of membrane–cortex rupture than does either single mutant. Cortexillin II helps maintain cortex–membrane connections and a wild type–like actin architecture (Shu *et al.*, 2012). In the context of a more-WT-like architecture, cortexillin I is essential for myosin II–mediated mechanosensitive accumulation.

Our results indicate that mechanical stress recruits kif12 and INCENP but not aurora kinase. On the basis of previous studies by De Lozanne's group, kif12 is required for the localization of INCENP at the cleavage furrow (Chen *et al.*, 2007). Both kif12 and INCENP are important for aurora kinase to target to the central spindle, which puts aurora at the bottom of this pathway (Li *et al.*, 2008). Of interest, myosin II is required for normal localization of aurora and INCENP during cytokinesis (Chen *et al.*, 2007; Li *et al.*, 2008). Consistently, we did not observe kif12 localization at the cleavage furrow of *myoII*-null cells (unpublished data). Therefore myosin II accumulation from mechanical stress, in addition to signals emanating from the spindle, can localize kif12 and INCENP as part of the mechanosensitive control system. Similarly, the actomyosin system, microtubules, and aurora B kinase ensure positive feedback of symmetry breaking in dividing mammalian cells (Hu *et al.*, 2008).

Kif12 and INCENP also play multiple roles in cytokinesis, particularly the abscission step and in recruiting myosin II when cells are challenged with mechanical stress. The *kif12*-null cells were previously reported to have problems accumulating myosin II at the cleavage furrow in unperturbed cells (Lakshmikanth *et al.*, 2004). However, we detected normal myosin II cleavage furrow accumulation in the two *kif12*-null cell lines (same lines used in Lakshmikanth *et al.*, 2004), as well as in *kif12* RNA interference cells when the cells were dividing unperturbed on surfaces (unpublished data). Because *kif12* mutants have severe cytokinesis defects, including a longer time to cytokinesis completion/failure, the interpretation of myosin II accumulation may be sensitive to image sampling frequency (i.e., phototoxicity may become a problem unless the time to complete cytokinesis is corrected for, which was not done in the work of Lakshmikanth *et al.*, 2004). Nevertheless, our observations that kif12 is part of a control system that tunes myosin II accumulation is in agreement with the main idea from Lakshmikanth *et al.* (2004), which is that kif12 participates in myosin II cleavage furrow accumulation.

Finally, the mechanosensory system has a natural shut-off mechanism. Because the myosin II/cortexillin I sensor depends on myosin II lever arm length (Ren *et al.*, 2009), this suggests that it is the isometric, cooperative actin-binding state of the myosin II motor that senses the stress (Tokuraku *et al.*, 2009; Luo *et al.*, 2012). As more myosin II heads accumulate, the average force/head decreases, allowing the heads to exit the cooperative actin-binding state. The myosin II heavy chain kinases then reset the level of myosin II assembly, maintaining the free pool of myosin II monomers (Yumura *et al.*, 2005; Luo *et al.*, 2012). Thus, implicit in the myosin II

mechanochemical and regulatory systems is the shut-off valve for the control system. Myosin II–based feedback control may be fundamental for other contractile systems such as those that drive tissue morphogenesis (Fernandez-Gonzalez *et al.*, 2009; He *et al.*, 2010) and focal adhesion maturation (Kuo *et al.*, 2011).

MATERIALS AND METHODS

Cell strains and culture

Dictyostelium discoideum strains used in this study are listed in Supplemental Table S1. All cells were cultured in enriched HL-5 media (1.4× HL-5 enriched with 8% FM) with penicillin and streptomycin at 22°C on 10-cm Petri dishes (Robinson and Spudich, 2000). Wild-type strains include KAx3, Ax3:Rep orf+ (HS1000), and rescued mutant strains (Ruppel *et al.*, 1994; Robinson and Spudich, 2000; Lee *et al.*, 2010). The *myoII* cells (Ruppel *et al.*, 1994); *iqgap1*, *iqgap2*, and *iqgap1/2* cells (Lee *et al.*, 2010); *cortI*, *cortII*, and *cortI/II* cells (Robinson and Spudich, 2000; Lee *et al.*, 2010); *kif12* cells (Lakshmikanth *et al.*, 2004); and *incenp* cells (Chen *et al.*, 2007) have been described previously. Where possible, strains were confirmed to have WT endogenous levels of myosin II, cortexillin I, and cortexillin II proteins (as appropriate). Wild-type and mutant strains were transformed with plasmids carrying fluorescently labeled genes of interest. All plasmids, RFP-tubulin, GFP-myosin II, citrine-WT myosin II, citrine-ΔBLCBS myosin II, GFP-IQGAP1, GFP-IQGAP2, GFP-cortexillin I, GFP-kif12, GFP-INCENP, and GFP-aurora, have also been described previously (Lakshmikanth *et al.*, 2004; Effler *et al.*, 2006; Chen *et al.*, 2007; Li *et al.*, 2008; Ren *et al.*, 2009; Lee *et al.*, 2010). GFP-rac1A and GFP-cortexillin II were prepared by amplifying both genes from a cDNA library and cloning into a modified version of the pDM181 vector, which includes a GFP-fusion insert. For control strains, cells were transformed with the empty vector and/or the DMSO carrier (for pharmacological experiments) as appropriate. In addition, only the matched parental strain and the rescued strain were considered as WT controls for each mutant cell line. Transformation was achieved by electroporation using a Genepulser-II electroporator (Bio-Rad, Hercules, CA). Transformed cells were selected with either 10–15 μg/ml G418 or 15-50 μg/ml hygromycin, or both drugs when two plasmids were transformed at once. Fluorescent reporters were confirmed to have similar expression levels (for the same reporter) across strains by comparing cytoplasmic fluorescence intensities.

Micropipette aspiration and cortical tension measurements

The instrumental and experimental setups were previously described in detail (Effler *et al.*, 2006). For the mechanosensing experiments, 0.2–0.5 nN/μm^2 of pressure was applied to the cell cortex with a micropipette (2–3 μm in radius, R_p). For cortical tension measurements, the aspiration pressure was increased to the equilibrium pressure (ΔP) in which the length of the cell inside the pipette (L_p) was equal to R_p. The effective cortical tension (T_{eff}) was determined by applying the Young–Laplace equation: $\Delta P = 2T_{eff}(1/R_p - 1/R_c)$, where R_c is the radius of the cell and ΔP is the equilibrium pressure when $L_p = R_p$ (Derganc *et al.*, 2000; Octtaviani *et al.*, 2006). For nocodazole experiments using MPA, cells were incubated overnight in HL-5 media with 0.2% DMSO (the nocodazole carrier) to eliminate the effects from DMSO treatment. Then a dividing cell was located and 10 μM nocodazole was added. The spindle marked with RFP-tubulin was monitored for about 5 min until the spindle disassembled, and then the dividing cell was aspirated. Nocodazole-treated cells were compared with DMSO-treated control cells.

Imaging and image analysis

For imaging, cells were transferred from Petri dishes to imaging chambers and allowed to adhere for 15 min in growth media. After the cells adhered, the growth media was gently replaced with 2-(*N*-morpholino)ethanesulfonic acid (MES) starvation buffer (50 mM MES, pH 6.8, 2 mM $MgCl_2$, 0.2 mM $CaCl_2$). For confocal imaging, a Zeiss 510 Meta with a 63× (numerical aperture [NA] 1.4) objective was used (Carl Zeiss, Jena, Germany). For all other studies, cell imaging was performed in a temperature-controlled room at 22°C with a motorized Olympus IX81 microscope using a 40× (NA 1.3) objective and a 1.6× optovar (Olympus, Center Valley, PA), as described previously (Effler *et al.*, 2006). ImageJ (National Institutes of Health, Bethesda, MD) was used for image analysis. Most cell strains were labeled with RFP- or GFP-tubulin to mark the mitotic spindle of the dividing cells. For the mechanosensing analysis, dividing cells were deformed by micropipette aspiration. For quantification, the logarithm of the ratio of the background-corrected mean pixel intensity of the cortex inside the pipette (I_p) to the opposite cortex outside the pipette (I_o) was determined, that is, $\log(I_p/I_o)$. For quantifying the myosin II furrow-to-pole intensity ratio, the average background-corrected pixel intensities of both sides of the furrow (I_f) and both of the poles (I_p) were measured. The furrow-to-pole intensity ratio (I_f/I_p) was calculated. The average background-corrected pixel intensities of the cytoplasm (I_c) were also measured so that ratios relative to cytoplasm could be determined. Please note that the term I_p is used in two different contexts, intensity in the pipette and intensity of the polar cortex.

For spindle morphology analysis, cells expressing GFP-kif12, GFP-tubulin, or RFP-tubulin were imaged and scored qualitatively for their spindle morphology. Cells with straight and symmetrically and centrally aligned spindles were considered to have normal morphology. Cells with curvy or asymmetrically displaced spindles were considered to have abnormal morphology.

Cleavage furrow-thinning analysis

The imaging and quantification methods were previously described in detail (Zhang and Robinson, 2005). In short, differential interference contrast movies of dividing cells were captured at 2-s intervals. Furrow diameter and length at each time point were measured using ImageJ. The point at which the furrow diameter (D_f) equaled the furrow length (L_f) yielded the crossover distance (D_x). For rescaling, the D_f was normalized by D_x and plotted against the shifted time axis, by which the time at which D_x was achieved was reset to 0 s.

Agarose overlay

Thin sheets of 2% agarose gel in sterile MES starvation buffer were prepared following the protocol developed by Fukui *et al.* (1986, 1987), which is available from dictyBase (http://dictybase.org). After cells settled in the imaging chambers for 15 min, the media in the imaging chamber was gently removed and replaced by MES starvation buffer. Thin agarose sheets were carefully placed on the surface of MES buffer. MES buffer was slowly and almost completely removed to allow the agarose sheet to directly press on the cells in the imaging chamber. To avoid potential complications of the imaging chamber drying due to evaporation, fresh imaging chambers were replaced every 15 min to ensure optimum conditions for cell behaviors. We confirmed the success of cytokinesis of the WT cells under these conditions. We found that 80% (22/28) of WT cells completed cytokinesis, which is only a little lower than the success rate (95–98%) for WT cells dividing unperturbed on surfaces (Effler *et al.*, 2006; Octtaviani *et al.*, 2006). For nocodazole treatment with agarose overlay, cells were cultured in HL-5 media with 0.2% DMSO overnight. During the experiment, a dividing cell was located, and

10 μM nocodazole was treated. The spindle was monitored until it disassembled, after which an agarose sheet was applied.

Statistical analyses

Data sets were collected and analyzed using KaleidaGraph (Synergy Software, Reading, PA). Analysis of variance (ANOVA) or Student's *t* tests were performed using KaleidaGraph. Comparison of proportions was performed with SE = $\sqrt{[f(1 - f)/n]}$, where f is the fraction of the population showing a behavior and n is the sample size. Only p values <0.05 were considered significant, and the calculated p values are included on the graphs, in the text, and/or in the figure legends.

ACKNOWLEDGMENTS

We thank Jim Spudich for the *kif12*-null cell lines, the GFP-kif12 expression construct, and discussions regarding myosin II localization the *kif12*-null cells. We thank Cathryn Kabacoff for help generating cell lines and the Robinson lab for helpful feedback on the manuscript. This work is supported by National Institutes of Health Grants GM066817 (to D.N.R.) and GM86704 (to D.N.R. and P.A.I.), American Cancer Society Grant RSG CCG-114122 (to D.N.R.), and an American Heart Association predoctoral fellowship (to Y.-S.K).

REFERENCES

Adachi H, Takahashi Y, Hasebe T, Shirouzu M, Yokoyama S, Sutoh K (1997). *Dictyostelium* IQGAP-related protein specifically involved in the completion of cytokinesis. J Cell Biol 137, 891–898.

Bosgraaf L, van Haastert PJ (2006). The regulation of myosin II in *Dictyostelium*. Eur J Cell Biol 85, 969–979.

Breckenridge MT, Dulyaninova NG, Egelhoff TT (2009). Multiple regulatory steps control mammalian nonmuscle myosin II assembly in live cells. Mol Biol Cell 20, 338–347.

Burgess DR, Chang F (2005). Site selection for the cleavage furrow at cytokinesis. Trends Cell Biol 15, 156–162.

Cabernard C, Prehoda KE, Doe CQ (2010). A spindle-independent cleavage furrow positioning pathway. Nature 467, 91–94.

Chen Q, Lakshmikanth GS, Spudich JA, DeLozanne A (2007). The localization of inner centromeric protein (INCENP) at the cleavage furrow is dependent on Kif12 and involves interactions of the N terminus of INCENP with the actin cytoskeleton. Mol Biol Cell 18, 3366–3374.

Cooke CA, Heck MM, Earnshaw WC (1987). The inner centromere protein (INCENP) antigens: movement from inner centromere to midbody during mitosis. J Cell Biol 105, 2053–2067.

Derganc J, Božic B, Svetina S, Žekš B (2000). Stability analysis of micropipette aspiration of neutrophils. Biophys J 79, 153–162.

Effler JC, Kee Y-S, Berk JM, Tran MN, Iglesias PA, Robinson DN (2006). Mitosis-specific mechanosensing and contractile protein redistribution control cell shape. Curr Biol 16, 1962–1967.

Egelhoff TT, Lee RJ, Spudich JA (1993). *Dictyostelium* myosin heavy chain phosphorylation sites regulate myosin filament assembly and localization in vivo. Cell 75, 363–371.

Faix J, Clougherty C, Konzok A, Mintert U, Murphy J, Albrecht R, Mühlbauer B, Kuhlmann J (1998). The IQGAP-related protein DGAP1 interacts with Rac and is involved in the modulation of the F-actin cytoskeleton and control of cell motility. J Cell Sci 111, 3059–3071.

Faix J, Steinmetz M, Boves H, Kammerer RA, Lottspeich F, Mintert U, Murphy J, Stock A, Aebi U, Gerisch G (1996). Cortexillins, major determinants of cell shape and size, are actin-bundling proteins with a parallel coiled-coil tail. Cell 86, 631–642.

Faix J, Weber I, Mintert U, Köhler J, Lottspeich F, Marriott G (2001). Recruitment of cortexillin into the cleavage furrow is controlled by Rac1 and IQGAP-related proteins. EMBO J 20, 3705–3715.

Fang X, Luo J, Nishihama R, Wloka C, Dravis C, Travaglia M, Iwase M, Vallen EA, Bi E (2010). Biphasic targeting and cleavage furrow ingression directed by the tail of a myosin II. J Cell Biol 191, 1333–1350.

Fenn WO (1923). A quantitative comparison between the energy liberated and the work performed by the isolated sartorius muscle of the frog. J Physiol 58, 175–203.

Fernandez-Gonzalez R, Simoes Sde M, Roper JC, Eaton S, Zallen JA (2009). Myosin II dynamics are regulated by tension in intercalating cells. Dev Cell 17, 736–743.

Fujiwara T, Bandi M, Nitta M, Ivanova EV, Bronson RT, Pellman D (2005). Cytokinesis failure generating tetraploids promotes tumorigenesis in p53-null cells. Nature 437, 1043–1047.

Fukata M, Watanabe T, Noritake J, Nakagawa M, Yamaga M, Kuroda S, Matsuura Y, Iwamatsu A, Perez F, Kaibuchi K (2002). Rac1 and Cdc42 capture microtubules through IQGAP1 and CLIP-170. Cell 109, 873–885.

Fukui Y, Yumura S, Yumura T (1987). Agar-overlay immunofluorescence: high-resolution studies of cytoskeletal components and their changes during chemotaxis. Methods Cell Biol 28, 347–356.

Fukui Y, Yumura S, Yumura T, Mori H (1986). Agar overlay method: high-resolution immunofluorescence for the study of the contractile apparatus. Methods Enzymol 134, 573–580.

Glotzer M (2005). The molecular requirements for cytokinesis. Science 307, 1735–1739.

Gupton SL, Waterman-Storer CM (2006). Spatiotemporal feedback between actomyosin and focal-adhesion systems optimizes rapid cell migration. Cell 125, 1361–1374.

He L, Wang X, Tang HL, Montell DJ (2010). Tissue elongation requires oscillating contractions of a basal actomyosin network. Nat Cell Biol 12, 1133–1142.

Hiramoto Y (1956). Cell division without mitotic apparatus in sea urchin eggs. Exp Cell Res 11, 630–636.

Hiramoto Y (1990). Mechanical properties of the cortex before and during cleavage. Ann N Y Acad Sci 582, 22–30.

Hu C, Coughlin M, Field CM, Mitchison TJ (2008). Cell polarization during monopolar cytokinesis. J Cell Biol 181, 195–202.

Huxley AF, Simmons RM (1971). Proposed mechanism of force generation in striated muscle. Nature 233, 533–538.

Kuo JC, Han X, Hsiao CT, Yates JR 3rd, Waterman CM (2011). Analysis of the myosin-II-responsive focal adhesion proteome reveals a role for beta-Pix in negative regulation of focal adhesion maturation. Nat Cell Biol 13, 383–393.

Lakshmikanth G, Warrick HM, Spudich JA (2004). A mitotic kinesin-like protein required for normal karyokinesis, myosin localization to the furrow, and cytokinesis in *Dictyostelium*. Proc Natl Acad Sci USA 101, 16519–16524.

Laporte D, Coffman VC, Lee IJ, Wu JQ (2011). Assembly and architecture of precursor nodes during fission yeast cytokinesis. J Cell Biol 192, 1005–1021.

Lee S, Shen Z, Robinson DN, Briggs S, Firtel RA (2010). Involvement of the cytoskeleton in controlling leading edge function during chemotaxis. Mol Biol Cell 21, 1810–1824.

Li H, Chen Q, Kaller M, Nellen W, Graf R, De Lozanne A (2008). *Dictyostelium* Aurora kinase has properties of both Aurora A and Aurora B kinases. Eukaryot Cell 7, 894–905.

Liu KK, Williams DR, Briscoe BJ (1996). Compressive deformation of a single microcapsule. Phys Rev E 54, 6673–6680.

Luo T, Mohan K, Srivastava V, Ren Y, Iglesias PA, Robinson DN (2012). Understanding the cooperative interactions between myosin II and actin crosslinkers mediated by actin filaments during mechanosensation. Biophys J 102, 238–247.

Mahajan RK, Vaughan KT, Johns JA, Pardee JD (1989). Actin filaments mediate *Dictyostelium* myosin assembly in vitro. Proc Natl Acad Sci USA 86, 6161–6165.

Mondal S, Burgute B, Rieger D, Muller R, Rivero F, Faix J, Schleicher M, Noegel AA (2010). Regulation of the actin cytoskeleton by an interaction of IQGAP related protein GAPA with filamin and cortexillin I. PLoS ONE 5, e15440.

Monod J, Changeux JP, Jacob F (1963). Allosteric proteins and cellular control systems. J Mol Biol 6, 306–329.

Octtaviani E, Effler JC, Robinson DN (2006). Enlazin, a natural fusion of two classes of canonical cytoskeletal proteins, contributes to cytokinesis dynamics. Mol Biol Cell 17, 5275–5286.

Orlova A, Egelman EH (1997). Cooperative rigor binding of myosin to actin is a function of F-actin structure. J Mol Biol 265, 469–474.

Ou G, Stuurman N, D'Ambrosio M, Vale RD (2010). Polarized myosin produces unequal-size daughters during asymmetric cell division. Science 330, 677–680.

Rappaport R (1996). Cytokinesis in Animal Cells, Cambridge: Cambridge University Press.

Reichl EM, Ren Y, Morphew MK, Delannoy M, Effler JC, Girard KD, Divi S, Iglesias PA, Kuo SC, Robinson DN (2008). Interactions between myosin and actin crosslinkers control cytokinesis contractility dynamics and mechanics. Curr Biol 18, 471–480.

Ren Y, Effler JC, Norstrom M, Luo T, Firtel RA, Iglesias PA, Rock RS, Robinson DN (2009). Mechanosensing through cooperative interactions between myosin II and the actin crosslinker cortexillin I. Curr Biol 19, 1421–1428.
Robinson DN (2010). 14-3-3, an integrator of cell mechanics and cytokinesis. Small GTPases 1, 165–169.
Robinson DN, Spudich JA (2000). Dynacortin, a genetic link between equatorial contractility and global shape control discovered by library complementation of a *Dictyostelium discoideum* cytokinesis mutant. J Cell Biol 150, 823–838.
Ruppel KM, Uyeda TQP, Spudich JA (1994). Role of highly conserved lysine 130 of myosin motor domain. In vivo and in vitro characterization of site specifically mutated myosin. J Biol Chem 269, 18773–18780.
Shu S, Liu X, Kriebel PW, Daniels MP, Korn ED (2012). Actin crosslinking proteins, cortexillin I and II, are required for cAMP-signaling during *Dictyostelium* chemotaxis and development. Mol Biol Cell 23, 390–400.
Stock A, Steinmetz MO, Janmey PA, Aebi U, Gerisch G, Kammerer RA, Weber I, Faix J (1999). Domain analysis of cortexillin I: actin-bundling, PIP_2-binding and the rescue of cytokinesis. EMBO J 18, 5274–5284.
Surcel A, Kee Y-S, Luo T, Robinson DN (2010). Cytokinesis through biochemical-mechanical feedback loops. Semin Cell Dev Biol 21, 866–873.
Takahashi K, Yamada T (1998). Application of an immune feedback mechanism to control systems. JSME Int J C 41, 184–191.
Tokuraku K, Kurogi R, Toya R, Uyeda TQP (2009). Novel mode of cooperative binding between myosin and Mg2+-actin filaments in the presence of low concentrations of ATP. J Mol Biol 386, 149–162.
Tucker DM, Williamson PA (1984). Asymmetric neural control systems in human self-regulation. Psychol Rev 91, 185–215.
Uehara R, Goshima G, Mabuchi I, Vale RD, Spudich JA, Griffis ER (2010). Determinants of myosin II cortical localization during cytokinesis. Curr Biol 20, 1080–1085.
Uyeda TQ, Iwadate Y, Umeki N, Nagasaki A, Yumura S (2011). Stretching actin filaments within cells enhances their affinity for the myosin II motor domain. PLoS ONE 6, e26200.
von Dassow G, Verbrugghe KJ, Miller AL, Sider JR, Bement WM (2009). Action at a distance during cytokinesis. J Cell Biol 187, 831–846.
Wolpert L (1966). The mechanical properties of the membrane of the sea urchin egg during cleavage. Exp Cell Res 41, 385–396.
Yumura S, Mori H, Fukui Y (1984). Localization of actin and myosin for the study of ameboid movement in *Dictyostelium* using improved immunofluorescence. J Cell Biol 99, 894–899.
Yumura S, Ueda M, Sako Y, Kitanishi-Yumura T, Yanagida T (2008). Multiple mechanisms for accumulation of myosin II filaments at the equator during cytokinesis. Traffic 9, 2089–2099.
Yumura S, Uyeda TQP (1997). Transport of myosin II to the equatorial region without its own motor activity in mitotic *Dictyostelium* cells. Mol Biol Cell 8, 2089–2099.
Yumura S, Yoshida M, Betapudi V, Licate LS, Iwadate Y, Nagasaki A, Uyeda TQ, Egelhoff TT (2005). Multiple myosin II heavy chain kinases: roles in filament assembly control and proper cytokinesis in *Dictyostelium*. Mol Biol Cell 16, 4256–4266.
Zang J-H, Spudich JA (1998). Myosin II localization during cytokinesis occurs by a mechanism that does not require its motor domain. Proc Natl Acad Sci USA 95, 13652–13657.
Zhang W, Robinson DN (2005). Balance of actively generated contractile and resistive forces controls cytokinesis dynamics. Proc Natl Acad Sci USA 102, 7186–7191.

A mechanosensory system governs myosin II accumulation in dividing cells

Yee-Seir Kee, Yixin Ren, Danielle Dorfman, Miho Iijima, Richard Firtel, Pablo A. Iglesias, and Douglas N. Robinson

Supplementary Materials

Supplementary Materials include Figures S1-S5 plus legends and Table S1.

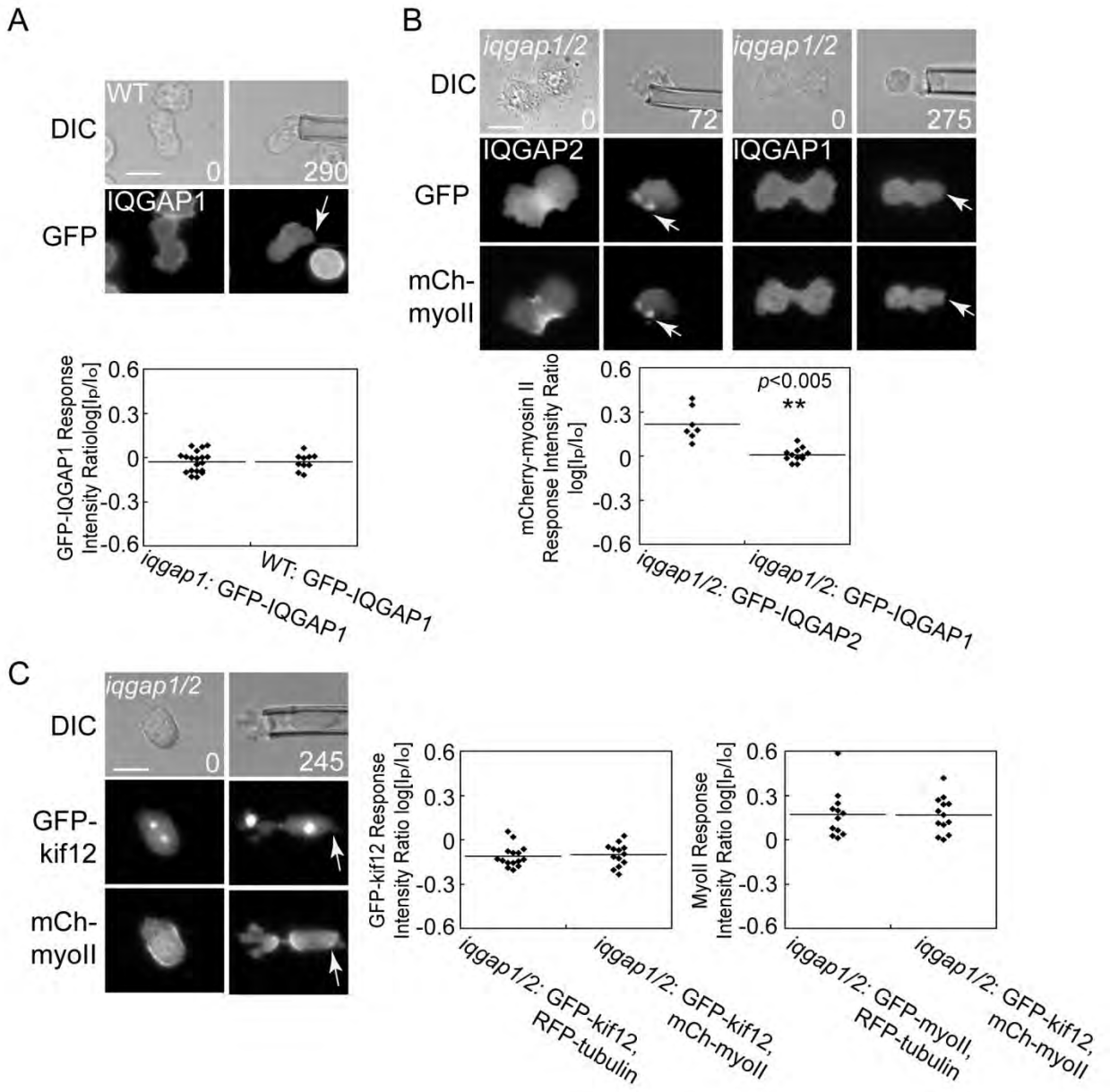

Figure S1. The roles of IQGAP1 and IQGAP2 in the mechanosensitivity of dividing cells.
(**A**) In a WT background, IQGAP1 did not accumulate at the micropipette (white arrows). The distribution of response intensity ratio was comparable in *iqgap1* cells rescued with GFP-IQGAP1 (data reproduced from Fig. 2A). Scale bars in A, B, and C represent 10 μm.
(**B**) Expression of IQGAP2 in the *iqgap1/2* null cells allowed myosin II mechanosensitive accumulation whereas expression of IQGAP1 in these cells inhibited the accumulation (ST: p=0.002).
(**C**) GFP-kif12 and mCherry (mCh)-myosin II were co-expressed in *iqgap1/2* mutant cells. Consistently, GFP-kif12 showed no accumulation at the micropipette, whereas mCh-myosin II exhibited mechanosensitive localization. The GFP-kif12 and mCh-myosin II response ratio distributions were not different from the kif12 responses in Fig. 4A and myosin II responses in Fig 3A.

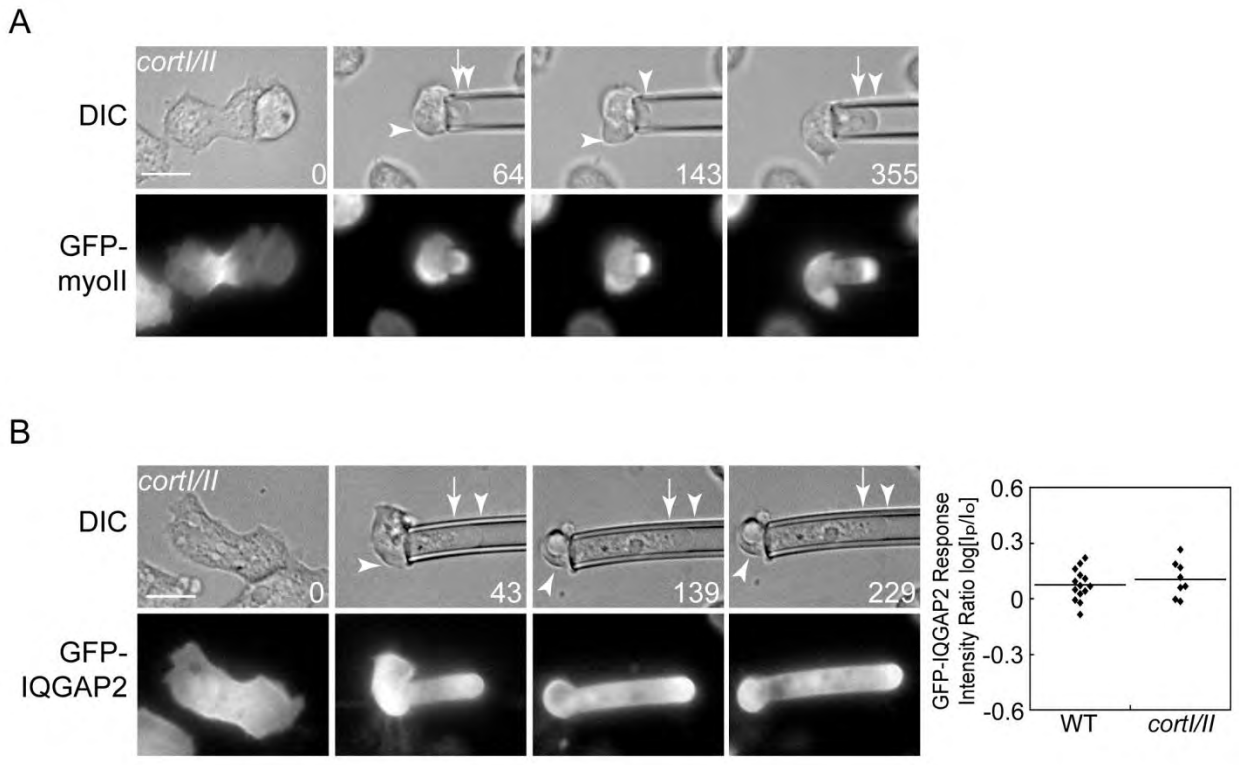

Figure S2. Cortical stability is disrupted in *cortI/II* mutant.
(**A**) Upon micropipette aspiration, *cortI/II* mutant showed apparent membrane detachment and blebs in regions inside and outside the pipette. The arrows indicate the position of cytoplasm and the arrow heads indicate the membrane. Myosin II accumulated at the blebbing regions. Scale bars in A and B represent 10 μm.
(**B**) Similar to myosin II, IQGAP2 localized to blebs in *cortI/II* cells. Although the dot plot shows no difference between IQGAP2 recruitment in WT and *cortI/II* mutant (ST: p=0.45), the behavior of recruitment is different. Time scale is in seconds.

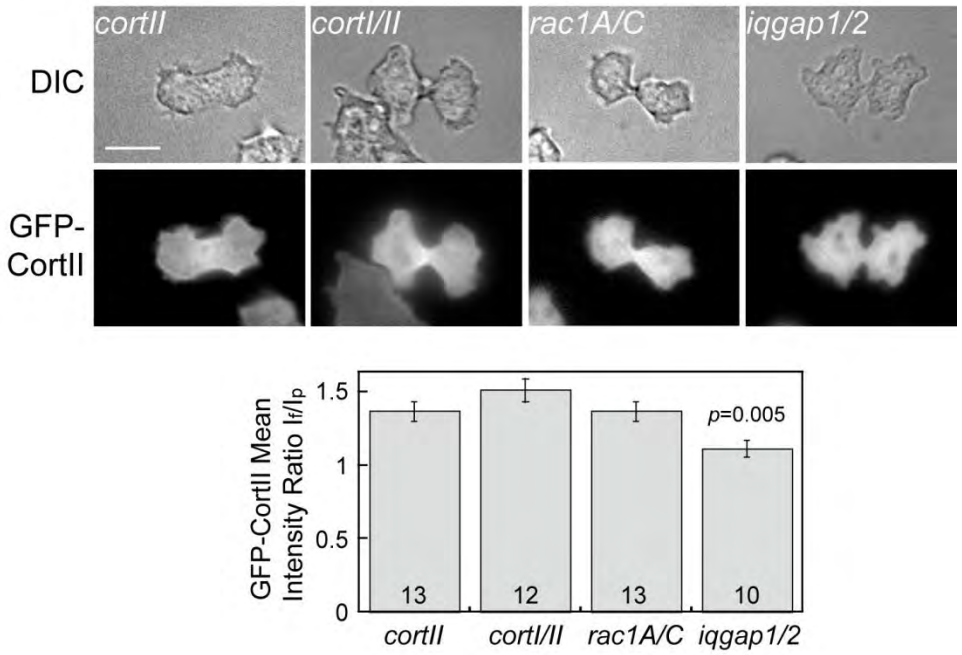

Figure S3. Cortexillin II cleavage furrow localization is reduced in *iqgap1/2* null cells. GFP-cortexillin II displayed cleavage furrow localization in *cortII*, *cortI/II*, and *rac1A/C* mutants. Cortexillin II levels were reduced in *iqgap1/2* mutants. Quantification of furrow to pole intensity ratio (I_f/I_p) and sample size are shown in the bar graph. Scale bar represents 10 µm.

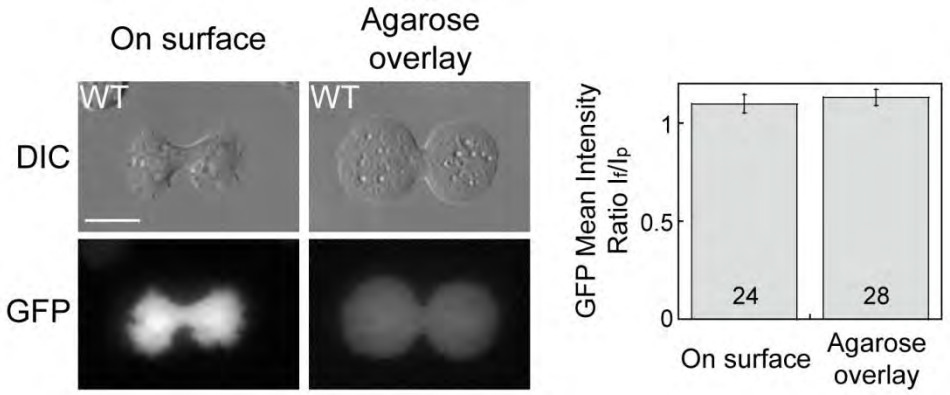

Figure S4. GFP furrow to pole mean intensity ratio is indistinguishable in dividing cells grown on surface or under agarose overlay.
WT cells expressing soluble GFP showed uniform cytoplasmic localization. The GFP I_f/I_p ratios of dividing cells grown on surface and compressed by agarose overlay are indistinguishable. Scale bar represents 10 μm.

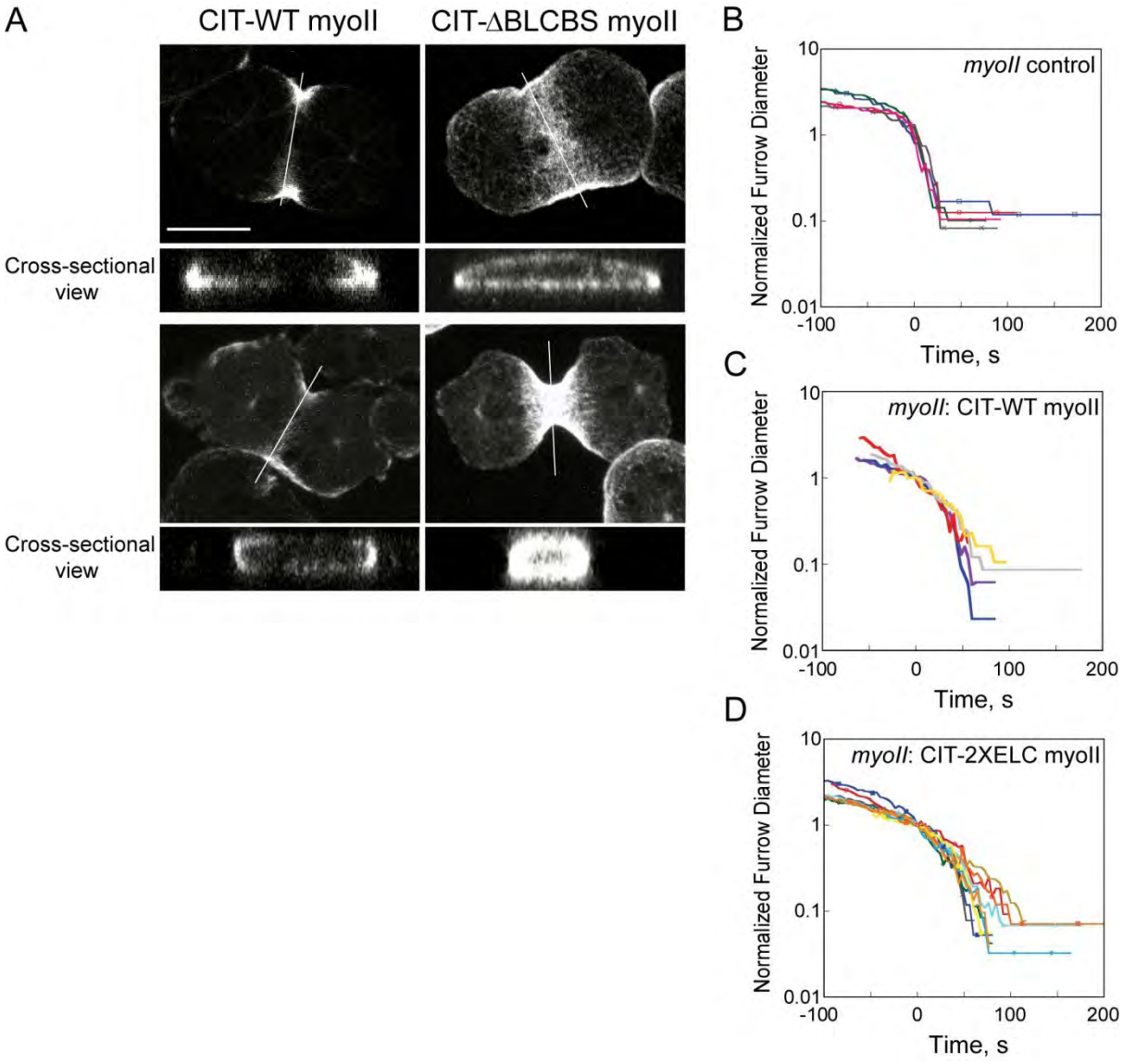

Figure S5. Myosin II lever-arm length is important for concentrating myosin II to the lateral edge furrow cortex and determining furrow ingression dynamics.
(**A**) *MyoII* cells expressing Citrine-labeled (CIT) WT myoII and CIT-ΔBLCBS myoII along with GFP-tubulin were imaged by confocal microscopy under agarose compression. CIT-WT myosin II strongly localized to the lateral cortex of the cleavage furrow. CIT-ΔBLCBS myoII did not show lateral cortex enrichment. Scale bar represents 10 μm.
(**B-D**) Unaveraged curves of the furrow-thinning dynamics of the *myoII* null cells and *myoII* null cells complemented with CIT-WT myosin II, or CIT-2xELC myosin II. The averaged curves are shown in Fig. 7D.

Table S1. Strains used in the study.

Strain	Genotype	Experimental Applications
myoII control	*myoII*(HS1)	Cleavage furrow thinning analysis
myoII: GFP-α-tubulin; Citrine-myoII	*myoII*(HS1)::Cit-myoII, Hyg^R:pDRH; GFP-α-tubulin, G418^R:pDEX	Cleavage furrow thinning analysis, unperturbed cytokinesis, agarose overlay, confocal imaging with agarose overlay
myoII: GFP-α-tubulin; Citrine-2XELC myoII	*myoII*(HS1)::Cit-2XELC myoII, Hyg^R:pDRH; GFP-α-tubulin, G418^R:pDEX	Cleavage furrow thinning analysis
myoII: GFP-α-tubulin; Citrine-ΔBLCBS myoII	*myoII*(HS1)::Cit-ΔBLCBSmyoII, Hyg^R:pDRH; GFP-α-tubulin, G418^R:pDEX	Cleavage furrow thinning analysis, agarose overlay, confocal imaging with agarose overlay
myoII: RFP-α-tubulin; GFP-kif12	*myoII*(HS1)::RFP-α-tubulin, Hyg^R:pDRH; GFP-kif12, G418^R:pTX	MPA (kif12 recruitment study)
myoII: RFP-α-tubulin; GFP-IQGAP2	*myoII*(HS1)::RFP-α-tubulin, Hyg^R:pDRH; GFP-IQGAP2, G418^R:pEXP4	MPA (IQGAP2 recruitment)
WT control	Ax3(Rep orf+)	MPA (cortical tension measurement), agarose overlay, unperturbed cytokinesis
WT: GFP	Ax3(Rep orf+)::GFP, Hyg^R:pDRH	Unperturbed cytokinesis, agarose overlay
WT: RFP-α-tubulin; GFP-myoII	Ax3(Rep orf+)::RFP-α-tubulin, Hyg^R:pDRH; GFP-myoII, G418^R:pBIG	Unperturbed cytokinesis, agarose overlay
WT: GFP-α-tubulin	Ax3(Rep orf+)::GFP-α-tubulin, Hyg^R:pDRH;	Spindle quality assessment
kif12	*kif12*(Rep orf+)	MPA (cortical tension measurement)
kif12: RFP-α-tubulin; GFP-myoII	*kif12*(Rep orf+)::RFP-α-tubulin, Hyg^R:pDRH; GFP-myoII, G418^R:pBIG	MPA (myoII recruitment), unperturbed cytokinesis, agarose overlay
kif12: mCh-myoII; GFP-kif12	*kif12*(Rep orf+)::mCh-myoII, Hyg^R:pDRH; GFP-kif12, G418^R:pTX	Agarose overlay
kif12: GFP-α-tubulin	*kif12*(Rep orf+)::GFP-α-tubulin, Hyg^R:pDRH;	Spindle quality assessment
WT control	KAx3(RF)	MPA (cortical tension measurement)
WT: RFP-α-tubulin; GFP-kif12	KAx3(RF)::RFP-α-tubulin, Hyg^R:pDRH; GFP-kif12, G418^R:pTX	MPA (kif12 recruitment), spindle quality assessment, kif12 cleavage furrow recruitment
WT: RFP-α-tubulin; GFP-myoII	KAx3(RF)::RFP-α-tubulin, Hyg^R:pDRH; GFP-myoII, G418^R:pBIG	MPA (myoII recruitment), agarose overlay
WT: RFP-α-tubulin; GFP-aurora	KAx3(RF)::RFP-α-tubulin, Hyg^R:pDRH; GFP-aurora, G418^R:pTX	MPA (aurora kinase recruitment)
WT: RFP-α-tubulin; GFP-rac1A	KAx3(RF)::RFP-α-tubulin, Hyg^R:pDRH; GFP-rac1A, G418^R:pDM181	MPA (Rac1A recruitment)
WT: RFP-α-tubulin; GFP-IQGAP1	KAx3(RF)::RFP-α-tubulin, Hyg^R:pDRH; GFP-IQGAP1, G418^R:pEXP4	MPA (IQGAP1 recruitment)
WT: RFP-α-tubulin; GFP-IQGAP2	KAx3(RF)::RFP-α-tubulin, Hyg^R:pDRH; GFP-IQGAP2, G418^R:pEXP4	MPA (IQGAP2 recruitment)
WT: mCh-myoII; GFP-IQGAP1	KAx3(RF)::mCh-myoII, Hyg^R:pDRH; GFP-IQGAP1, G418^R:pEXP4	MPA (myoII recruitment)
WT: GFP	KAx3(RF):: Hyg^R:pDRH; GFP, G418^R:pDM181	MPA (GFP recruitment as control)
WT: GFP-kif12; mCherry	KAx3(RF)::mCherry, Hyg^R:pDRH; GFP-kif12, G418^R:pTX	MPA (kif12 recruitment and mCherry recruitment as control)
iqgap1	*iqgap1*(RF)	MPA (cortical tension measurement)
iqgap1: RFP-α-tubulin; GFP-IQGAP1	*iqgap1*(RF)::RFP-α-tubulin, Hyg^R:pDRH; GFP-IQGAP1, G418^R:pEXP4	MPA (IQGAP1 recruitment)
iqgap1: RFP-α-tubulin; GFP-myoII	*iqgap1*(RF)::RFP-α-tubulin, Hyg^R:pDRH; GFP-myoII, G418^R:pBIG	MPA (myoII recruitment), unperturbed cytokinesis, agarose overlay

iqgap1: RFP-α-tubulin; GFP-cortI	*iqgap1*(RF)::RFP-α-tubulin, Hyg^R:pDRH; GFP-cortI, G418^R:pEXP4	MPA (cortI recruitment)
iqgap1: RFP-α-tubulin; GFP-kif12	*iqgap1*(RF)::RFP-α-tubulin, Hyg^R:pDRH; GFP-kif12, G418R:pTX	Spindle quality assessment, kif12 cleavage furrow recruitment
iqgap2	*iqgap2*(RF)	MPA (cortical tension measurement)
iqgap2: RFP-α-tubulin; GFP-IQGAP2	*iqgap2*(RF)::RFP-α-tubulin, Hyg^R:pDRH; GFP-IQGAP2, G418^R:pEXP4	MPA (IQGAP2 recruitment)
iqgap2: RFP-α-tubulin; GFP-myoII	*iqgap2*(RF)::RFP-α-tubulin, Hyg^R:pDRH; GFP-myoII, G418^R:pBIG	MPA (myoII recruitment), unperturbed cytokinesis, agarose overlay
iqgap2: RFP-α-tubulin; GFP-cortI	*iqgap2*(RF)::RFP-α-tubulin, Hyg^R:pDRH; GFP-cortI, G418^R:pEXP4	MPA (cortI recruitment)
iqgap2: RFP-α-tubulin; GFP-kif12	*iqgap2*(RF)::RFP-α-tubulin, Hyg^R:pDRH; GFP-kif12, G418^R:pTX	MPA (kif12 recruitment), spindle quality assessment, kif12 cleavage furrow recruitment
iqgap2: mCh-myoII; GFP-IQGAP2	*iqgap2*(RF)::mCh-myoII, Hyg^R:pDRH; GFP-IQGAP2, G418^R:pEXP4	MPA (myoII recruitment), agarose overlay
iqgap1/2	*iqgap1/2*(RF)	MPA (cortical tension measurement)
iqgap1/2: RFP-α-tubulin; GFP-myoII	*iqgap1/2*(RF)::RFP-α-tubulin, Hyg^R:pDRH; GFP-myoII, G418^R:pBIG	MPA (myoII recruitment), unperturbed cytokinesis, agarose overlay
iqgap1/2: RFP-α-tubulin; GFP-kif12	*iqgap1/2*(RF)::RFP-α-tubulin, Hyg^R:pDRH; GFP-kif12, G418^R:pTX	MPA (kif12 recruitment), unperturbed cytokinesis, agarose overlay
iqgap1/2: mCh-myoII; GFP-IQGAP2	*iqgap1/2*(RF)::mCh-myoII, Hyg^R:pDRH; GFP-IQGAP2, G418^R:pEXP4	MPA (myoII recruitment)
iqgap1/2: mCh-myoII; GFP-IQGAP1	*iqgap1/2*(RF)::mCh-myoII, Hyg^R:pDRH; GFP-IQGAP1, G418^R:pEXP4	MPA (myoII recruitment)
iqgap1/2: mCh-myoII; GFP-kif12	*iqgap1/2*(RF)::mCh-myoII, Hyg^R:pDRH; GFP-kif12, G418^R:pTX	MPA (myoII and kif12 recruitment)
iqgap1/2: RFP-α-tubulin; GFP-cortI	*iqgap1/2*(RF)::RFP-α-tubulin, Hyg^R:pDRH; GFP-cortI, G418^R:pEXP4	MPA (cortI recruitment)
iqgap1/2: RFP-α-tubulin; GFP-cortII	*iqgap1/2*(RF)::RFP-α-tubulin, Hyg^R:pDRH; GFP-cortII, G418^R:pDM181	CortII cleavage furrow localization
cortI	*cortI*(RF)	MPA (cortical tension measurement)
cortI: RFP-α-tubulin; GFP-IQGAP2	*cortI*(RF)::RFP-α-tubulin, Hyg^R:pDRH; GFP-IQGAP2, G418^R:pEXP4	MPA (IQGAP2 recruitment)
cortI: RFP-α-tubulin; GFP-myoII	*cortI*(RF)::RFP-α-tubulin, Hyg^R:pDRH; GFP-myoII, G418^R:pBIG	Unperturbed cytokinesis, agarose overlay
cortII	*cortII*(RF)	MPA (cortical tension measurement)
cortII: RFP-α-tubulin; GFP-cortII	*cortII*(RF)::RFP-α-tubulin, Hyg^R:pDRH; GFP-cortII, G418^R:pDM181	MPA (cortII recruitment), cortII cleavage furrow localization
cortII: RFP-α-tubulin; GFP-myoII	*cortII*(RF)::RFP-α-tubulin, Hyg^R:pDRH; GFP-myoII, G418^R:pBIG	MPA (myoII recruitment), unperturbed cytokinesis, agarose overlay
cortI/II	*cortI/II*(RF)	MPA (cortical tension measurement)
cortI/II: RFP-α-tubulin; GFP-cortI	*cortI/II*(RF)::RFP-α-tubulin, Hyg^R:pDRH; GFP-cortI, G418^R:pDM181	MPA (cortI recruitment)
cortI/II: RFP-α-tubulin; GFP-cortII	*cortI/II*(RF)::RFP-α-tubulin, Hyg^R:pDRH; GFP-cortI, G418^R:pDM181	CortII cleavage furrow localization
cortI/II: RFP-α-tubulin; GFP-myoII	*cortI/II*(RF)::RFP-α-tubulin, Hyg^R:pDRH; GFP-cortII, G418^R:pDM181	MPA (myoII recruitment), unperturbed cytokinesis, agarose overlay
cortI/II: RFP-α-tubulin; GFP-IQGAP2	*cortI/II*(RF)::RFP-α-tubulin, Hyg^R:pDRH; GFP-IQGAP2, G418^R:pEXP4	MPA (IQGAP2 recruitment)

rac1A/C: RFP-α-tubulin; GFP-myoII	*rac1A/C*(MI)::RFP-α-tubulin, Hyg^R:pDRH; GFP-myoII, G418^R:pBIG	MPA (myoII recruitment)

rac1A/C: RFP-α-tubulin; GFP-myoII	*rac1A/C*(MI)::RFP-α-tubulin, Hyg^R:pDRH; GFP-myoII, $G418^R$:pBIG	MPA (cortI recruitment)
rac1A/C: RFP-α-tubulin; GFP-cortII	*rac1A/C*(MI)::RFP-α-tubulin, Hyg^R:pDRH; GFP-cortII, $G418^R$:pDM181	CortII cleavage furrow localization

incenp	*incenp*(AD)	MPA (cortical tension measurement)
incenp: RFP-α-tubulin; GFP-INCENP	*incenp*(AD)::RFP-α-tubulin, Hyg^R:pDRH; GFP-INCENP, $G418^R$:pTX	MPA (INCENP recruitment, cortical tension measurement)
incenp: RFP-α-tubulin; GFP-myoII	*incenp*(AD)::RFP-α-tubulin, Hyg^R:pDRH; GFP-myoII, $G418^R$:pBIG	MPA (myoII recruitment), unperturbed cytokinesis, agarose overlay
incenp: mCH-myoII; GFP-INCENP	*incenp*(AD)::mCH-myoII, Hyg^R:pDRH; GFP-INCENP, $G418^R$:pTX	MPA (myoII recruitment), unperturbed cytokinesis, agarose overlay